

Multi-IRS-Aided Doppler-Tolerant Wideband DFRC System

Tong Wei, *Student Member, IEEE*, Linlong Wu, *Member, IEEE*, Kumar Vijay Mishra, *Senior Member, IEEE*, M. R. Bhavani Shankar, *Senior Member, IEEE*

Abstract—Intelligence reflecting surface (IRS) is recognized as the enabler of future dual-function radar-communications (DFRC) for improving spectral efficiency, coverage, parameter estimation, and interference suppression. Prior studies on IRS-aided DFRC focus on either narrowband processing, single-IRS deployment, static targets, non-clutter scenario, or under-utilized line-of-sight (LoS) and non-line-of-sight (NLoS) paths. In this paper, we address the aforementioned shortcomings by optimizing a wideband DFRC system that comprises multiple IRSs and a dual-function base station that jointly processes the LoS and NLoS wideband multi-carrier signals to extract communications symbols and moving target parameters in the presence of clutter. We formulate the transmit and IRS beamformer design as the maximization of the worst-case radar signal-to-interference-plus-noise ratio (SINR) subject to transmit power and communications SINR. We tackle this nonconvex problem under the alternating optimization framework, where the subproblems are solved by a combination of Dinkelbach algorithm, consensus alternating direction method of multipliers, and Riemannian steepest descent. Our numerical experiments show that the proposed multi-IRS-aided wideband DFRC provides over 6 dB radar SINR and 40% improvement in target detection over a single-IRS system.

Index Terms—Dinkelbach algorithm, dual-function radar-communications, intelligence reflecting surfaces, non-line-of-sight sensing, wideband beamforming.

I. INTRODUCTION

Over the past few years, intelligent reflecting surface (IRS) has emerged as a promising technology to achieve a smart wireless environment that allows enhanced coverage, security, and interference suppression [2–4]. An IRS comprises a large number of low-cost sub-wavelength passive meta-material elements, each of which is able to independently control the phase of the impinging signal and hence shape the radiation beampattern to alter the radio propagation environment [2, 5, 6]. The near passive behavior implies potential for large-scale IRS deployment without additional energy consumption when compared with the conventional relays [7, 8]. These characteristics of IRS have attracted considerable attention in both sensing [9–12] and communications communities [5, 6, 13, 14].

Initial investigations of IRS were limited to wireless communications to enhance, for instance, the coverage, spectral efficiency, energy saving, secrecy rate, and interference suppression; see e.g. [5] and references therein. These studies utilized IRS to compensate for the end-to-end (transmitter-IRS-receiver) path loss [15, 16]. Further, the base station (BS) and reflecting surfaces employed, respectively, active and largely passive beamformers [17, 18], which may be designed jointly. For example, the IRS-aided channel in [19] is estimated for each reflecting element using pilot symbols followed by transmit precoder design. In [20], IRS was employed to minimize the total transmit power while guaranteeing the signal-to-interference-plus-noise ratio (SINR) among all users. Some recent studies [21] employ IRS to correctly estimate the position and orientation of the mobile user to improve the quality-of-service (QoS). The system model in all of these investigations employed a single IRS thereby

limiting the flexibility of deployment and the degrees-of-freedom for resolving the large-scale channel fading.

Multiple IRSs, if optimally deployed, have the potential to exploit the multiplicative beamforming gain to further enhance the QoS [22–28]. For example, in secure communications [22], IRS is useful in establishing a favorable propagation environment, wherein the sum rate of legitimate users is maximized under the constraint on leakage of information to the potential eavesdroppers. Note that [22] ignores the interaction between the IRSs, thus simplifying the design and analysis. When the line-of-sight (LoS) path between the BS and users is blocked, the double IRS system has been shown to yield the virtual LoS in multi-user multiple-input multiple-output (MIMO) communications [26]. A multi-IRS-aided wireless communications system developed in [28] leverages short-distance LoS channel between two adjacent IRSs to receive the transmit message via multiple reflections. These multi-IRS studies are limited their analyses to only the non-line-of-sight (NLoS) path between the transmitter and receiver via IRS.

The investigations into the potential of IRS toward enhancing the performance of, primarily, MIMO radars followed the spurt of IRS research in communications [9, 10, 12, 14, 37–41]. The focus of these works has been similar to IRS-aided communications, i.e. use IRS to aid the radar in detecting NLoS targets. There is a rich heritage of research on non-IRS-based NLoS radar; see e.g. [42, 43] and references therein. However, these systems require prior and accurate knowledge of the environment and geometry (such as walls and buildings). Further, unlike an IRS-assisted system, they are unable to alter and control the wireless media. This makes IRS very attractive for remote sensing of hidden or blocked objects. In [9], IRS facilitated coverage extension of an NLoS radar. This was extended to monostatic/bistatic and LoS/NLoS radar systems in [37] and the receive signal-to-noise ratio (SNR) was maximized by optimizing the phase-shifts. This study revealed that, when the IRS is far away from the radar transmitter or receiver, the detection performance has only marginal gain. A very recent study in [38] considered multiple IRSs to enhance the transmit power toward target-of-interest with constraints on the clutter backscatter.

Lately, there has been significant interest in characterizing IRS performance for integrated sensing and communications (ISAC) systems [30, 33–36, 44–47]. The motivation for developing ISAC systems lies in addressing the increasing spectrum congestion by designing common hardware and waveforms for both radar and communications [48–51]. These dual-function radar-communications (DFRC) units [52] have the advantages of resource sharing, hardware cost and energy efficiency. A single-IRS-aided DFRC proposed in [30] was radar-centric in that it maximized the radar SNR while utilizing the reflecting surface to simultaneously facilitate the target detection and single-user communications. This was extended to multiple users in [35], in which the radar transmit beampattern was synthesized and followed by minimization of multi-user interference (MUI) to guarantee the communications QoS. While several theoretical works assume the IRS phase-shifts to be continuous-valued, in practice, the shifts only admit discrete/quantized values. This aspect was analyzed in the IRS-aided DFRC system suggested in [36]. A few other recent studies on communications-centric DFRC design, where the IRS

The authors are with the Interdisciplinary Centre for Security, Reliability and Trust (SnT), University of Luxembourg, Luxembourg City L-1855, Luxembourg. E-mail: {tong.wei@, linlong.wu@, kumar.mishra@ext., bhavani.shankar@}uni.lu.

The conference precursor of this paper appeared in the 2022 IEEE International Hybrid Symposium on Joint communications & Sensing (JC&S) [1].

TABLE I
COMPARISON WITH THE STATE-OF-THE-ART

cf.	Radar	Communications	IRS; Phases	Targets; Clutter	Radar paths ^a	Users	Design metric
[29]	PA ^b	SC-SISO ^c	Double; Continuous	Static, multiple; Yes	LoS, NLoS	Single	Communications SINR
[30]	MIMO	SC-MIMO ^d	Single; Continuous	Static, single; No	LoS, NLoS	Single	Radar SNR
[31]	MIMO	SC-MIMO	Single; Continuous	Static, single; No	LoS, NLoS	Multiple	Detection probability
[32]	MIMO	SC-MIMO	Single; Continuous	Static, single; Yes	LoS, NLoS	Multiple	Radar SINR
[33]	MIMO	SC-MIMO	Single; Continuous	Static, single; Yes	LoS	Multiple	Sum-rate
[34]	MIMO	SC-MIMO	Single; Continuous	Static, multiple; No	LoS	Multiple	Transmit power
[35]	MIMO	SC-MIMO	Single; Continuous	Static, multiple; No	LoS	Multiple	Beampattern, MUI
[36]	MIMO	SC-MIMO	Single; Discrete	Static, multiple; No	LoS, NLoS	Multiple	Beampattern, MUI
This paper	W-MIMO ^e	MIMO-OFDM	Multiple; Continuous	Moving, single; Yes	LoS, NLoS	Multiple	Radar SINR

^a The communications system utilizes the LoS and NLoS paths in all these works. ^b PA: phased-array.

^c SC-SISO: single-carrier single-input-single-output. ^d SC-MIMO: single-carrier MIMO. ^e W-MIMO: wideband MIMO.

facilitates in maximizing secrecy rates [53, 54].

Nearly all of the aforementioned single-IRS-assisted DFRC approaches focus on a stationary target and narrowband transmission. While the former is an impractical assumption from radar perspective, the latter limits the application to lower frequency bands. Further, single IRS formulations limit the coverage region and ignore the spatial diversity of target radar cross-section (RCS). To address these shortcomings of prior research, in this paper, we propose utilizing multiple IRSs to assist a wideband DFRC system. In particular, we employ orthogonal frequency-division multiplexing (OFDM) waveform to detect a moving target and communicate with multiple users. We devise a Doppler filter bank against an unknown Doppler shift at the radar receiver. We show that by properly designing the transmit beamforming, phase-shift matrix, and Doppler filter-bank, we maximize the average radar SINR over all subcarriers while ensuring that the average SINR among all users is greater than a predetermined threshold, thus guaranteeing the communications QoS. Table I summarizes the key differences between our work and some major closely-related prior studies.

Preliminary results of this work appeared in our conference publication [1], where we introduced wideband IRS-assisted DFRC but ignored the LoS paths for both sensing and communications, did not consider moving target, and omitted detailed performance evaluations. In this work, we include these critical assumptions and our main contributions are:

1) Wideband IRS-aided DFRC. We propose a more comprehensive multi-IRS-aided wideband OFDM-DFRC model, which includes moving target in the radar scene and multiple single-antenna users for communications. We also consider both LoS and NLoS paths for radar and communications. The wideband design allows for varying beamformer weights with respect to subcarrier frequencies and thereby offset the beam squint effect [55, 56]. Our proposed system, therefore, subsumes current stationary target, narrowband, non-IRS, or single-IRS DFRC studies [30, 32, 57]; also, see Table I.

2) Doppler-tolerant IRS-DFRC. Analogous to a Doppler filter bank in a conventional radar receiver, we design multiple receive filters to maximize the worst-case radar SINR accounting for all possible Doppler slices. This robust design is subjected to the constraints of subcarrier transmit power and the minimum communications SINR among all users. We then solve the resulting nonconvex maximin problem, which involves fractional quartic objective function accompanied by the difference of convex (DC) and unimodular constraints.

3) Alternating optimization (AO) for joint design. We develop an alternating maximization (AM) framework to tackle the above nonconvex problem. We first utilize the semidefinite relaxation (SDR) to obtain the closed-form solution for the Doppler filter bank design. Then, we combine the Dinkelbach and majorization method to tackle the transmit beamformer design subproblem. Finally, the consensus alternating direction of multipliers (C-ADMM) [58] and Riemannian steepest descent (RSD) [35] approaches are jointly used to approxi-

mately solve the subproblem of phase-shift design.

4) Extensive performance evaluation. We validate our model and methods through comprehensive numerical experiments. Our proposed method achieves an enhanced radar SINR over its non-IRS, single-IRS, and narrowband counterparts. Our theoretical analyses and experimental investigation of the proposed IRS-aided DFRC reveal a trade-off between the communications and radar performance.

The remainder of this paper is organized as follows. In the next section, we introduce the signal model and problem formulation for multi-IRS-aided wideband DFRC system. In Section III, we develop our AM-based algorithm to tackle the formulated optimization problem, in which the corresponding subproblems are solved iteratively. We evaluate our methods in Section IV through extensive numerical examples. We conclude in Section V.

Throughout this paper, vectors and matrices are denoted by lower case boldface letter and upper case boldface letter, respectively. The notations $(\cdot)^T$, $(\cdot)^*$ and $(\cdot)^H$ denote the operations of transpose, conjugate, and Hermitian transpose, respectively; \mathbf{I}_L and $\mathbf{1}_L$ denote the $L \times L$ identity matrix and all-ones vector of length L , respectively; \otimes is the Kronecker product; $\Re(\cdot)$ and $\Im(\cdot)$ represent the real and imaginary parts of a complex number, respectively; $\text{vec}(\cdot)$ is the vectorization of its matrix argument; $\text{diag}(\cdot)$ and $\text{blkdiag}(\cdot)$ denote the diagonal and block diagonal matrix, respectively; $|\cdot|$, $\|\cdot\|_2$ and $\|\cdot\|_F$ represent the magnitude, ℓ_2 -norm, and Frobenius-norm, respectively; $(\cdot)^{(n)}$ denotes the value of the variable at the n -th outer iteration; and $\nabla(\cdot)$ and $\text{grad}(\cdot)$ are the Euclidean and Riemannian gradient operator, respectively.

II. SYSTEM MODEL AND PROBLEM FORMULATION

Consider a multi-IRS-aided wideband OFDM-DFRC system consisting of a dual-function transmitter, a colocated radar receiver, and M IRSs (Fig. 1). We denote the reflecting elements of m -th IRS, the number of antennas at the dual-function transmitter and the radar receiver by N_m , N_t and N_r , respectively. The transmitter and receiver are closely deployed with the dual-function base station (DFBS). The uniform inter-element spacings for the DFBS transmit and receive arrays are d_t and d_r , respectively. The IRS-aided DFRC system aims to detect a moving target against Q clutter patches while simultaneously serving U downlink (DL) single-antenna users in a two-dimensional (2-D) Cartesian plane. Assume that the DFBS, radar target, q -th clutter patch and m -th IRS are located at the coordinates, respectively, $\mathbf{p}_d = [x_d, y_d]$, $\mathbf{p}_t = [x_t, y_t]$, $\mathbf{p}_{c_q} = [x_{c_q}, y_{c_q}]$ and $\mathbf{p}_m = [x_{i_m}, y_{i_m}]$.

A. Transmit signal

The normalized transmit data symbol at the k -th subcarrier is $\mathbf{s}_k = [s_{k,1}, \dots, s_{k,U}]^T \in \mathbb{C}^{U \times 1}$, where $k = 1, \dots, K$ and $\mathbb{E}\{\mathbf{s}_k \mathbf{s}_k^H\} = \mathbf{I}_U$. Meanwhile, the data symbol is modulated and spread over K OFDM subcarriers. In the wideband OFDM system, the transmit steering vectors at different subcarriers are changed with

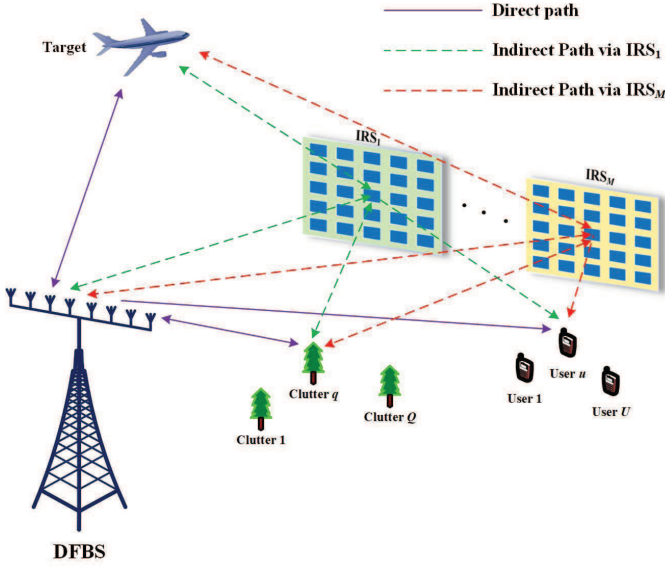


Fig. 1. Simplified illustration of a multi-IRS-aided wideband DFRC system.

the corresponding frequencies which lead to the beam-squint effect [56]. To mitigate this, we utilize a frequency-dependent beamforming technique to preprocess the transmit data symbol s_k in the frequency-domain. For the k -th subcarrier, denote the digital beamforming matrix by $\mathbf{F}_k = [\mathbf{f}_{k,1}, \dots, \mathbf{f}_{k,U}] \in \mathbb{C}^{N_t \times U}$, then the transmitted signal becomes $\mathbf{F}_k \mathbf{s}_k \in \mathbb{C}^{N_t \times 1}$. Applying the N_t K -point inverse fast Fourier transform (IFFT) to the frequency-domain signal $\mathbf{F}_k \mathbf{s}_k$, the transmit baseband signal at time instant t is

$$\mathbf{x}_T(t) = [x_1(t), \dots, x_{N_t}(t)]^T = \sum_{k=1}^K \mathbf{F}_k \mathbf{s}_k e^{j2\pi f_k t}, t \in (0, \Delta t), \quad (1)$$

where Δt denotes the OFDM duration exclusive of the cyclic prefix (CP) with length D , $f_k = (k-1)\Delta f$ denotes the baseband frequency at the k -th subcarrier and Δf is the frequency step of OFDM signaling. To guarantee the orthogonality of the subcarriers, the frequency spacing is set to $\Delta f = 1/\Delta t$. Meanwhile, for wideband DFRC, the total transmit power should meet the system requirement. In order to fully utilize the bandwidth, herein, we assume the transmit power satisfies $\|\mathbf{F}_k\|_F^2 \leq \mathcal{P}_k$, where \mathcal{P}_k denotes the maximum transmit power assigned to the k -th subcarrier. The baseband signal is then upconverted for transmission: $\mathbf{x}(t) = \mathbf{x}_T(t)e^{j2\pi f_c t}$, where f_c denotes the carrier frequency.

B. Channel and operating conditions

For radar system, we assume the transmit signal impinges on the target located at \mathbf{p}_t moving with velocity $\mathbf{v} = [v_x, v_y]$, where v_x and v_y are the velocity components along with x -axis and y -axis, respectively. The transmit signal is then reflected back from both direct and indirect paths to the radar receiver. Here, we consider the echoes coming via the following paths: Tx-target-Rx (**path 1** or the **direct path**), Tx-IRS-target-Rx (**path 2**), Tx-target-IRS-Rx (**path 3**), and Tx-IRS-target-IRS-Rx (**path 4**).

Denote the direct path channel coefficient of radar that includes path loss and target reflectivity by α_1 . The Doppler frequency of the target with respect to the direct path is $f_{D,1}$. The target angle of arrival/departure (AoA/AoD) with respect to DFBS is θ_t^1 . The propagation delay for the path between the DFBS and the target, the

¹Hereafter, all the AoAs/AoDs are measured with respect to the array broadside direction and are positive when moving clockwise.

differential propagation delay for the n_t -th transmitter with respect to the reference (first) transmitter, and the differential propagation delay for the n_r -th receiver with respect to the reference (first) receiver are, respectively,

$$\tau_{d,t} = \frac{\|\mathbf{p}_t - \mathbf{p}_d\|_2}{c}, \quad \tau_{n_t} = \frac{(n_t - 1)d_t \sin \theta_t}{c}, \quad \text{and} \quad \tau_{n_r} = \frac{(n_r - 1)d_r \sin \theta_t}{c}, \quad (2)$$

where $c = 3 \times 10^8$ m/s is the speed of light and θ_t denotes the target's AoA/AoD. Hence, the total time delay from the n_t -th transmitter and n_r -th receiver via **direct path** is

$$\tau_{\text{dir},n_r,n_t} = 2\tau_{d,t} + \tau_{n_t} + \tau_{n_r}. \quad (3)$$

Similarly, the propagation delays from the DFBS to m -th IRS and target to m -th IRS are $\tau_{d,i_m} = \frac{\|\mathbf{p}_d - \mathbf{p}_{i_m}\|_2}{c}$ and $\tau_{t,i_m} = \frac{\|\mathbf{p}_t - \mathbf{p}_{i_m}\|_2}{c}$, respectively. The total delay of indirect target path 2 from the n_t -th DFBS transmit antenna to the n_r -th DFBS receive antenna through the n_m -th element of the m -th IRS is $\tau_{\text{ind},m,2,n_m,n_t,n_r}$. This includes the differential path delays induced by the uniform linear array configuration of the DFBS and IRS.

Then, the Doppler frequencies with respect to the paths 1, 2, 3, and 4 are, respectively, [59]

$$f_{D,1} = \frac{f_c}{c} \left(\frac{\langle \mathbf{v}, \mathbf{p}_t - \mathbf{p}_d \rangle}{\|\mathbf{p}_t - \mathbf{p}_d\|_2} + \frac{\langle \mathbf{v}, \mathbf{p}_t - \mathbf{p}_d \rangle}{\|\mathbf{p}_t - \mathbf{p}_d\|_2} \right), \quad (4)$$

$$f_{D,m,2} = \frac{f_c}{c} \left(\frac{\langle \mathbf{v}, \mathbf{p}_t - \mathbf{p}_d \rangle}{\|\mathbf{p}_t - \mathbf{p}_d\|_2} + \frac{\langle \mathbf{v}, \mathbf{p}_t - \mathbf{p}_{i_m} \rangle}{\|\mathbf{p}_t - \mathbf{p}_{i_m}\|_2} \right), \quad \forall m, \quad (5)$$

$$f_{D,m,3} = \frac{f_c}{c} \left(\frac{\langle \mathbf{v}, \mathbf{p}_t - \mathbf{p}_d \rangle}{\|\mathbf{p}_t - \mathbf{p}_d\|_2} + \frac{\langle \mathbf{v}, \mathbf{p}_t - \mathbf{p}_{i_m} \rangle}{\|\mathbf{p}_t - \mathbf{p}_{i_m}\|_2} \right), \quad \forall m, \quad (6)$$

and

$$f_{D,m,4} = \frac{f_c}{c} \left(\frac{\langle \mathbf{v}, \mathbf{p}_d - \mathbf{p}_{i_m} \rangle}{\|\mathbf{p}_d - \mathbf{p}_{i_m}\|_2} + \frac{\langle \mathbf{v}, \mathbf{p}_d - \mathbf{p}_{i_m} \rangle}{\|\mathbf{p}_d - \mathbf{p}_{i_m}\|_2} \right), \quad \forall m. \quad (7)$$

We make following assumptions about the IRS-aided DFRC and channel parameters:

- A1** "Known channel state information (CSI)": The CSI matrix from the transmitter (or IRSs) to users are estimated in advance.
- A2** "Bandwidth-invariant Doppler": The bandwidth of OFDM signal is much smaller than the carrier frequency, i.e., $K\Delta f \ll f_c$. Hence, the phase-shifts arising from the Doppler effect are identical over all subcarriers.
- A3** "Constant Doppler shifts": The Doppler frequency of target does not change during each OFDM symbol duration $K\Delta t$, i.e., $dv_t/dt \ll c/(2f_c(\Delta t)^2)$.
- A4** "Constant IRS phase-shifts": The phase-shift of IRS is constant at different subcarriers: $\Phi_m(f_k) \approx \Phi_m, m = 1, \dots, M$ over all subcarrier frequencies f_k . The mutual interaction between various IRSs is negligible.

C. Radar receiver

The received signal from the target at the n_r -th radar antenna via **direct path** is a delayed, modulated, and scaled version of the transmit signal (1), that is,

$$s_{\text{dir},n_r}(t) = \sum_{n_t=1}^{N_t} \alpha_1 x_{n_t}(t - \tau_{\text{dir},n_r,n_t}) e^{j2\pi f_c(t - \tau_{\text{dir},n_r,n_t})} e^{j2\pi f_{D,1}(t - \tau_{\text{dir},n_r,n_t})}. \quad (8)$$

Stacking the echoes for all receive antennas and removing carrier frequency $e^{j2\pi f_c t}$, the $N_r \times 1$ baseband signal vector is

$$\mathbf{s}_{\text{dir}}(t) = [s_{\text{dir},1}(t), \dots, s_{\text{dir},N_r}(t)]^T = \sum_{k=1}^K \tilde{\alpha}_{1,k} \mathbf{a}_r(\theta_t, f_k) \mathbf{a}_t^T(\theta_t, f_k) \mathbf{F}_k \mathbf{s}_k e^{j2\pi f_k t}, \quad (9)$$

where $\tilde{\alpha}_{1,k} = \alpha_1 e^{j2\pi f_{D,1} \Delta t} e^{-j2\pi(f_c + f_k)2\tau_{d,t}}$ denotes the complex-value channel gain in terms of RCS, path loss, Doppler shift and propagation delay², $\mathbf{a}_r(\theta, f_k) \in \mathbb{C}^{N_r \times 1}$ and $\mathbf{a}_t(\theta, f_k) \in \mathbb{C}^{N_t \times 1}$ are the space-frequency steering vector of the dual-function transmitter and radar receiver expressed, respectively, as

$$\begin{aligned} \mathbf{a}_t(\theta, f_k) &= [1, e^{-jv_t(\theta, f_k)}, \dots, e^{-j(N_t-1)v_t(\theta, f_k)}]^T, \\ \mathbf{a}_r(\theta, f_k) &= [1, e^{-jv_r(\theta, f_k)}, \dots, e^{-j(N_r-1)v_r(\theta, f_k)}]^T, \end{aligned} \quad (10)$$

where $v_{t,r}(\theta, f_k) = 2\pi(f_k + f_c)(\frac{d_{t,r} \sin(\theta)}{c})$ denote the spatial-frequency shift. Sampling (9) at the rate $K/\Delta t$ within the symbol duration yields the $N_r \times 1$ vector

$$\begin{aligned} \mathbf{s}_{\text{dir}}[\tilde{n}] &= [\mathbf{s}_{\text{dir}_1}[\tilde{n}], \dots, \mathbf{s}_{\text{dir}_{N_r}}[\tilde{n}]]^T \\ &= \sum_{k=1}^K \tilde{\alpha}_{1,k} \mathbf{a}_r(\theta_t, f_k) \mathbf{a}_t^T(\theta_t, f_k) \mathbf{F}_k \mathbf{s}_k e^{j2\pi f_k \frac{\tilde{n}\Delta t}{K}}, \end{aligned} \quad (11)$$

where $\tilde{n} = 1, \dots, K$ denotes the discrete-time sample index. Combining all K samples, (11) in the matrix form is

$$\mathbf{S}_{\text{dir}} = [\mathbf{s}_{\text{dir}}[1], \dots, \mathbf{s}_{\text{dir}}[K]] \in \mathbb{C}^{N_r \times K}. \quad (12)$$

Applying K -point FFT to each row of (12) yields the $N_r \times 1$ frequency-domain vector for the k -th subcarrier as

$$\tilde{\mathbf{s}}_{\text{dir}}[f_k] = \mathbf{A}_{\text{dir},k} \mathbf{F}_k \mathbf{s}_k, \quad (13)$$

where $\mathbf{A}_{\text{dir},k} = \tilde{\alpha}_{1,k} \mathbf{a}_r(\theta_t, f_k) \mathbf{a}_t^T(\theta_t, f_k)$ is the direct channel response on the k -th subcarrier.

For the indirect path, note that IRS is modeled as a linear array in a 2-D plane. This can be easily extended to 3-D geometry by modifying the corresponding steering vector [44]. For the indirect path 2, i.e., the path traversing DFBS-IRS-Target-DFBS, we use the channel coefficient $\alpha_{m,2}$, which includes the path gain, target RCS and the phase shifts of the m th IRS. The received signal for path 2 is

$$\begin{aligned} \mathbf{s}_{\text{ind},m,2,n_r}(t) &= \sum_{n_t=1}^{N_t} \alpha_{m,2} \sum_{n_m=1}^{N_m} x_{n_t}(t - \tau_{\text{ind},m,2,n_m,n_t,n_r}) \\ &\times e^{j2\pi f_c(t - \tau_{\text{ind},m,p,q,2,n_t})} e^{j2\pi f_{D,2}(t - \tau_{\text{ind},m,2,n_m,n_t,n_r})} e^{j\phi_{m,n_m}}, \end{aligned} \quad (14)$$

where ϕ_{m,n_m} denotes the phase shift of the n_m -th element of the m -th IRS. Then, *mutatis mutandis*, the expressions for the indirect paths 3 and 4 are obtained. The overall indirect path signal via the m -th IRS is a superposition of all three paths, i.e.,

$$\mathbf{s}_{\text{ind},m,n_r}(t) = \mathbf{s}_{\text{ind},m,2,n_r}(t) + \mathbf{s}_{\text{ind},m,3,n_r}(t) + \mathbf{s}_{\text{ind},m,4,n_r}(t). \quad (15)$$

As in the direct path processing, after downconverting the indirect path receive signal, we similarly combine some terms with the channel gains to obtain new coefficients corresponding to the indirect paths 2, 3, and 4 of the m -th IRS as, respectively, $\tilde{\alpha}_{m,2} = \alpha_{m,2} e^{j2\pi f_{D,m,2} \Delta t} e^{-j2\pi(f_c + f_k)(\tau_{d,i_m} + \tau_{t,i_m} + \tau_{d,t})}$, $\tilde{\alpha}_{m,3} = \alpha_{m,3} e^{j2\pi f_{D,m,3} \Delta t} e^{-j2\pi(f_c + f_k)(\tau_{d,i_m} + \tau_{t,i_m} + \tau_{d,t})}$, and $\tilde{\alpha}_{m,4} = \alpha_{m,4} e^{j2\pi f_{D,m,4} \Delta t} e^{-j2\pi(f_c + f_k)(2\tau_{d,i_m} + 2\tau_{t,i_m})}$. The channel matrices for the paths m -th IRS-target-Rx, m -th IRS-Rx, Tx-target- m -th IRS, Tx- m -th IRS, and m -th IRS-target- m -th IRS are, respectively,

$$\mathbf{E}_{m,k} = \mathbf{a}_r(\theta_t, f_k) \mathbf{b}_m^T(\theta_{t,i_m}, f_k), \quad \mathbf{D}_{m,k} = \mathbf{a}_r(\theta_{i_m}, f_k) \mathbf{b}_m^T(\theta_{d,i_m}, f_k), \quad (16)$$

$$\mathbf{B}_{m,k} = \mathbf{b}_m(\theta_{t,i_m}, f_k) \mathbf{a}_t^T(\theta_t, f_k), \quad \mathbf{G}_{m,k} = \mathbf{b}_m(\theta_{d,i_m}, f_k) \mathbf{a}_t^T(\theta_{i_m}, f_k), \quad (17)$$

and $\mathbf{W}_{m,k} = \mathbf{b}_m(\theta_{t,i_m}, f_k) \mathbf{b}_m^T(\theta_{t,i_m}, f_k)$, where θ_{i_m} , θ_{t,i_m} and θ_{d,i_m} denote the angle of m -th IRS with respect to DFBS,

²Herein, the complex-valued term $e^{-j2\pi f_{D,1} \tau_d}$ is omitted because $f_{D,1} \tau_d = \text{const.}/c^2 \approx 0$.

target, and DFBS with respect to m -th IRS, respectively. The space-frequency steering vector of m -th IRS is $\mathbf{b}_m(\theta, f_k) = [1, e^{-jv_m(\theta, f_k)}, \dots, e^{-j(N_m-1)v_m(\theta, f_k)}]^T$.

We exploit the similarities between (14) and (8) to omit the intermediate steps and present the resulting simplified models in the sequel. It follows from (13) that, in frequency-domain, the received signal at k -th subcarrier via direct path is the product of the channel response matrix $\mathbf{A}_{\text{dir},k}$ and the frequency-dependent signal $\mathbf{F}_k \mathbf{s}_k$. Therefore, the $N_r \times 1$ received signal vector for all N_r receive antennas via indirect path assisted by the m -th IRS in the frequency-domain is

$$\begin{aligned} \tilde{\mathbf{s}}_{\text{ind},m}[f_k] &= (\tilde{\alpha}_{m,2} \mathbf{E}_{m,k} \mathbf{\Phi}_m \mathbf{G}_{m,k} + \tilde{\alpha}_{m,3} \mathbf{D}_{m,k} \mathbf{\Phi}_m \mathbf{B}_{m,k} \\ &\quad + \tilde{\alpha}_{m,4} \mathbf{D}_{m,k} \mathbf{\Phi}_m \mathbf{W}_{m,k} \mathbf{\Phi}_m \mathbf{G}_{m,k}) \mathbf{F}_k \mathbf{s}_k, \end{aligned} \quad (18)$$

where $\mathbf{\Phi}_m = \text{diag}(e^{j\phi_{m,1}}, \dots, e^{j\phi_{m,N_m}})$ denotes the phase-shift matrix of m -th IRS. Using the superposition principle, we obtain the receive signal across all M IRSs as

$$\tilde{\mathbf{s}}_{\text{ind}}[f_k] = \sum_{m=1}^M \tilde{\mathbf{s}}_{\text{ind},m}[f_k] = \mathbf{A}_{\text{ind},k}(\mathbf{\Phi}) \mathbf{F}_k \mathbf{s}_k, \quad (19)$$

where $\mathbf{A}_{\text{ind},k}(\mathbf{\Phi}) = \sum_{m=1}^M (\tilde{\alpha}_{m,2} \mathbf{E}_{m,k} \mathbf{\Phi}_m \mathbf{G}_{m,k} + \tilde{\alpha}_{m,3} \mathbf{D}_{m,k} \mathbf{\Phi}_m \mathbf{B}_{m,k} + \tilde{\alpha}_{m,4} \mathbf{D}_{m,k} \mathbf{\Phi}_m \mathbf{W}_{m,k} \mathbf{\Phi}_m \mathbf{G}_{m,k})$ denotes the indirect IRS-aided channel response and $\mathbf{\Phi} \in \{\mathbf{\Phi}_1, \dots, \mathbf{\Phi}_M\}$.

Similarly, the response matrices of the clutter scatterers for the paths m -IRS-DFBS, DFBS- m -IRS, and m -IRS-clutters- m -IRS, respectively, are $\tilde{\mathbf{E}}_{m,k} = \sum_{q=1}^Q \mathbf{a}_r(\theta_{c_q}, f_k) \mathbf{b}_m^T(\theta_{c_q, i_m}, f_k)$, $\tilde{\mathbf{B}}_{m,k} = \sum_{q=1}^Q \mathbf{b}_m(\theta_{c_q, i_m}, f_k) \mathbf{a}_t^T(\theta_{c_q}, f_k)$, and $\tilde{\mathbf{W}}_{m,k} = \sum_{q=1}^Q \mathbf{b}_m(\theta_{c_q, i_m}, f_k) \mathbf{b}_m^T(\theta_{c_q, i_m}, f_k)$. Hence, in the frequency-domain, the echo signal of the clutters via direct and indirect path are

$$\begin{aligned} \tilde{\mathbf{c}}_{\text{dir}}[f_k] &= \sum_{q=1}^Q \beta_1 \mathbf{a}_r(\theta_{c_q}, f_k) \mathbf{a}_t^T(\theta_{c_q}, f_k) \mathbf{F}_k \mathbf{s}_k = \tilde{\mathbf{A}}_{\text{dir},k} \mathbf{F}_k \mathbf{s}_k, \\ \tilde{\mathbf{c}}_{\text{ind}}[f_k] &= \sum_{m=1}^M \beta_2 \tilde{\mathbf{E}}_{m,k} \mathbf{\Phi}_m \mathbf{G}_{m,k} + \beta_3 \mathbf{D}_{m,k} \mathbf{\Phi}_m \tilde{\mathbf{B}}_{m,k} \\ &\quad + \beta_4 \mathbf{D}_{m,k} \mathbf{\Phi}_m \tilde{\mathbf{W}}_{m,k} \mathbf{\Phi}_m \mathbf{G}_{m,k} \mathbf{F}_k \mathbf{s}_k = \tilde{\mathbf{A}}_{\text{ind},k}(\mathbf{\Phi}) \mathbf{F}_k \mathbf{s}_k, \end{aligned}$$

where $\beta_1, \beta_2, \beta_3$ and β_4 are the corresponding channel gain of clutter scatterers.

Notice that from (4)-(7) the Doppler frequency is linearly proportional to the target velocity. We discretize the Doppler grid into P points so that the target velocity at any p -th grid point is $v_p \in [0, v_{\text{max}}]$, $p = 1, \dots, P$, where v_{max} is the maximum unambiguous velocity of the radar detection. Following (4)-(7), denote the respective Doppler slices or shifts corresponding to discretized velocity grid by $f_{D,1,p}$, $f_{D,m,2,p}$, $f_{D,m,3,p}$, and $f_{D,m,4,p}$. The composite received radar signal from both direct and indirect paths at p -th Doppler slice is

$$\tilde{\mathbf{y}}_{R,p}[f_k] = \tilde{\mathbf{s}}_{\text{dir},p}[f_k] + \tilde{\mathbf{s}}_{\text{ind},p}[f_k] + \tilde{\mathbf{c}}_{\text{dir}}[f_k] + \tilde{\mathbf{c}}_{\text{ind}}[f_k] + \tilde{\mathbf{n}}_R[f_k], \quad (20)$$

where $\tilde{\mathbf{n}}_R[f_k] \in \mathbb{C}^{N_r \times 1}$ denotes the radar noise at the k -th subcarrier with zero mean and covariance $\sigma_R^2 \mathbf{I}_{N_r}$. From (20), the average SINR of radar for the p -th Doppler slice is

$$\begin{aligned} \text{SINR}_{R,p} &= \frac{\sum_{k=1}^K |\mathbf{w}_p^H (\tilde{\mathbf{s}}_{\text{dir},p}[f_k] + \tilde{\mathbf{s}}_{\text{ind},p}[f_k])|^2}{\sum_{k=1}^K |\mathbf{w}_p^H (\tilde{\mathbf{c}}_{\text{dir}}[f_k] + \tilde{\mathbf{c}}_{\text{ind}}[f_k])|^2 + K \sigma_R^2 \mathbf{w}_p^H \mathbf{w}_p} \\ &= \frac{\sum_{k=1}^K \|\mathbf{w}_p^H (\mathbf{A}_{\text{dir},k,p} + \mathbf{A}_{\text{ind},k,p}(\mathbf{\Phi})) \mathbf{F}_k\|_2^2}{\sum_{k=1}^K \|\mathbf{w}_p^H (\tilde{\mathbf{A}}_{\text{dir},k} + \tilde{\mathbf{A}}_{\text{ind},k}(\mathbf{\Phi})) \mathbf{F}_k\|_2^2 + K \sigma_R^2 \mathbf{w}_p^H \mathbf{w}_p}, \end{aligned} \quad (21)$$

where \mathbf{w}_p , $p = 1 \dots, P$ denotes the Doppler filter bank.

D. Communications receiver

Following the wideband channel model [60], we denote the CSI from transmitter and m -th IRS to u -th user at the k -th subcarrier, respectively, by

$$\mathbf{h}_{u,k} = \sum_{l=1}^L \sum_{k=1}^K \alpha_l e^{-j\frac{2\pi k d}{K}} \mathbf{a}_t(\phi_l, f_k) r(kT_s - \tau_l), \in \mathbb{C}^{N_t \times 1}, \quad (22)$$

and

$$\mathbf{h}_{u,m,k} = \sum_{l_m=1}^{L_m} \sum_{k=1}^K \alpha_{l_m} e^{-j\frac{2\pi k d}{K}} \mathbf{a}_t(\phi_{l_m}, f_k) r(kT_s - \tau_{l_m}), \in \mathbb{C}^{N_m \times 1}, \quad (23)$$

where α_l and α_{l_m} are the channel gains; L and L_m are the number of clusters; τ_l and τ_{l_m} are the path delays; ϕ_l , and ϕ_{l_m} denote the the AoDs of all clusters; and $r(t)$ is the raised-cosine function that takes into account the effect of Nyquist filters employed at the transmitter and receiver to avoid the intersymbol interference as, $r(t) = \sum_{k=-\infty}^{+\infty} \delta(t - kK/\Delta T) = \delta(t)$.

Standard methods are available to estimate the CSI [56, 61, 62]. Hence, in this work, assume CSI is known/estimated *a priori*. The receive signal of the users at the k -th subcarrier is [58]

$$y_{C_u}(t) = \sum_{k=1}^K (\mathbf{h}_{u,k}^T \mathbf{F}_k \mathbf{s}_k e^{j2\pi f_k t} + \sum_{m=1}^M \mathbf{h}_{u,m,k}^T \Phi_m \mathbf{G}_{m,k} \mathbf{F}_k \mathbf{s}_k e^{j2\pi f_k t} + n_{C_u}(t)), \quad (24)$$

where $n_{C_u}(t)$ denotes the u -th users' complex white Gaussian noise with zero mean and covariance $\Delta t \sigma_C^2 \mathbf{I}_U$. Sampling (24) at the rate $K/\Delta t$ within the symbol duration, we obtain

$$y_{C_u}[\tilde{n}] = \sum_{k=1}^K (\mathbf{h}_{u,k} \mathbf{F}_k \mathbf{s}_k e^{j2\pi f_k \frac{\tilde{n}\Delta t}{K}} + \sum_{m=1}^M \mathbf{h}_{u,m,k} \Phi_m \mathbf{G}_{m,k} \mathbf{F}_k \mathbf{s}_k e^{j2\pi f_k \frac{\tilde{n}\Delta t}{K}} + n_{C_u}[\tilde{n}]), \quad (25)$$

where $\tilde{n} = 1, \dots, K$ is the discrete-time sample index and synchronized with the radar receiver. Applying K -point FFT along the index \tilde{n} , the receive signal of u -th user at k -th subcarrier is

$$\begin{aligned} \tilde{y}_{C_u}[f_k] &= \underbrace{\mathbf{h}_{u,k}^T \mathbf{f}_{k,u} \mathbf{s}_{k,u}}_{\text{desired signal}} + \underbrace{\sum_{i \neq u} \mathbf{h}_{u,k}^T \mathbf{f}_{k,i} \mathbf{s}_{k,i} + \sum_{i \neq u, m=1}^M \mathbf{h}_{u,m,k}^T \Phi_m \mathbf{G}_{m,k} \mathbf{f}_{k,i} \mathbf{s}_{k,i}}_{\text{MUI}} + \tilde{n}_{C_u}[f_k], \end{aligned} \quad (26)$$

where $\mathbf{f}_{k,u}$ denotes the u -th column of \mathbf{F}_k and $\tilde{n}_{C_u}[f_k]$ denotes the additional noise of u -th user at the k -th subcarrier with zero mean and variance σ_C^2 .

We define Λ_u as the diagonal matrix with u -th diagonal element is one and the others are zero. Following (26), the average signal power of the u -th user over all K subcarriers is

$$\mathcal{P}_u = \frac{1}{K} \sum_{k=1}^K \left\| \mathbf{h}_{u,k}^T + \underbrace{\sum_{m=1}^M \mathbf{h}_{u,m,k}^T \Phi_m \mathbf{G}_{m,k}}_{\mathbf{z}_{u,k}(\Phi)} \mathbf{F}_k \Lambda_u \right\|_2^2. \quad (27)$$

Similarly, defining $\bar{\Lambda}_u$ as the diagonal matrix with u -th diagonal element is zero and the others are one, the average power of MUI at the u -th user is $\mathcal{P}_{\text{MUI}} = \frac{1}{K} \sum_{k=1}^K \left\| (\mathbf{h}_{u,k}^T +$

$\sum_{m=1}^M \mathbf{h}_{u,m,k}^T \Phi_m \mathbf{G}_{m,k}) \mathbf{F}_k \bar{\Lambda}_u \right\|_2^2$. The average communications SINR of the u -th users is

$$\begin{aligned} \text{SINR}_{C_u} &= \frac{\sum_{k=1}^K \|(\mathbf{h}_{u,k}^T + \mathbf{z}_{u,k}(\Phi)) \mathbf{F}_k \Lambda_u\|_2^2}{\sum_{k=1}^K \|(\mathbf{h}_{u,k}^T + \mathbf{z}_{u,k}(\Phi)) \mathbf{F}_k \bar{\Lambda}_u\|_2^2 + K\sigma_C^2} \\ &= \frac{\sum_{k=1}^K \|\text{vec}(\mathbf{F}_k)^H (\Lambda_u \otimes (\mathbf{h}_{u,k}^T + \mathbf{z}_{u,k}(\Phi))^H)\|_2^2}{\sum_{k=1}^K \|\text{vec}(\mathbf{F}_k)^H (\bar{\Lambda}_u \otimes (\mathbf{h}_{u,k}^T + \mathbf{z}_{u,k}(\Phi))^H)\|_2^2 + K\sigma_C^2}, \end{aligned} \quad (28)$$

where $\mathbf{z}_{u,k}(\Phi) = \sum_{m=1}^M \mathbf{h}_{u,m,k}^T \Phi_m \mathbf{G}_{m,k}$ denotes the multi-IRS-aided channel of communication.

E. Joint design problem

Our goal is to design the transmit beamformers \mathbf{F}_k , IRS phase-shifts Φ_m , and receive filter bank \mathbf{w}_p that maximize the minimum radar SINR over different Doppler slices while guaranteeing the communications SINR of all users. The resulting optimization problem is

$$\underset{\mathbf{w}_p, \Phi_m, \mathbf{F}_k}{\text{maximize}} \quad \min_p \{\text{SINR}_{R_p}\} \quad (29a)$$

$$\text{subject to} \quad \|\mathbf{F}_k\|_F^2 \leq \mathcal{P}_k, \forall k, \quad (29b)$$

$$\text{SINR}_{C_u} \geq \xi, \forall u, \quad (29c)$$

$$|\Phi_m(i, i)| = 1, \forall i, \forall m, \quad (29d)$$

where $|\Phi_m(i, i)| = 1$ denotes the unimodular constraint over all elements of IRS phase-shift matrices and ξ is the threshold of communications SINR. The problem in (29) is highly nonconvex because of the maximin objective function, difference of convex (DC), and constant modulus constraints. Hence, it is difficult to obtain a closed-form solution.

III. ALTERNATING OPTIMIZATION

Even without the nonconvex constraints (29c) and (29d), the optimization problem in (29) is still nonconvex with respect to \mathbf{w}_p , Φ_m and \mathbf{F}_k because of the fractional maximin objective function. Thus, the global optimal solution is intractable [63]. Meanwhile, all the design variables including the Doppler filter bank, wideband beamformer and IRS phase-shifts are also coupled. Therefore, we resort to the AO framework [64], also known as block coordinate descent, to decouple the design problems of the Doppler filter bank, wideband beamformer, and phase-shifts. Then, the corresponding subproblems are approximately solved in each iteration. This optimization framework also has the flexibility to apply various update order of the blocks updates to this algorithm. More importantly, if each subproblem is solved optimally or suboptimally so that the objective value is improved, then the monotonicity of AO could be guaranteed. For a lower bounded objective function in a minimization problem, this monotonicity will ensure the convergence [58, 63].

A. Doppler filter bank design

Denote the signal covariance matrices of clutter and target at the p -th Doppler slice, respectively, by $\Upsilon_c = \sum_{k=1}^K (\tilde{\mathbf{A}}_{\text{dir},k} + \tilde{\mathbf{A}}_{\text{ind},k}(\Phi)) \mathbf{F}_k \mathbf{F}_k^H (\tilde{\mathbf{A}}_{\text{dir},k} + \tilde{\mathbf{A}}_{\text{ind},k}(\Phi))^H$ and $\Upsilon_{p,t} = \sum_{k=1}^K (\mathbf{A}_{p,\text{dir},k} + \mathbf{A}_{p,\text{ind},k}(\Phi)) \mathbf{F}_k \mathbf{F}_k^H (\mathbf{A}_{p,\text{dir},k} + \mathbf{A}_{p,\text{ind},k}(\Phi))^H$. Thus, for a given transmit beamforming \mathbf{F}_k and phase-shift Φ_m , the subproblem to obtain Doppler filter bank \mathbf{w}_p is

$$\underset{\mathbf{w}_1, \dots, \mathbf{w}_P}{\text{maximize}} \quad \min_p \frac{\mathbf{w}_p^H \Upsilon_{p,t} \mathbf{w}_p}{\mathbf{w}_p^H \Upsilon_c \mathbf{w}_p + K\sigma_R^2 \mathbf{w}_p^H \mathbf{w}_p}. \quad (30)$$

Note that the objective function of problem (30) is separable in terms of the variables $\mathbf{w}_p, p = 1, \dots, P$. Hence, we obtain an optimal solution for the maximin problem (30) by solving the following P disjoint problems

$$\underset{\mathbf{w}_p}{\text{maximize}} \quad \frac{\mathbf{w}_p^H \Upsilon_{p,t} \mathbf{w}_p}{\mathbf{w}_p^H \tilde{\Upsilon}_c \mathbf{w}_p}, \quad (31)$$

where $p = 1, \dots, P$ and $\tilde{\Upsilon}_c = \Upsilon_c + K\sigma_R^2 \mathbf{I}$. Using the Charnes-Cooper transformation [65], we convert (31) to an equivalent problem

$$\underset{\mathbf{w}_p}{\text{minimize}} \quad \mathbf{w}_p^H \tilde{\Upsilon}_c \mathbf{w}_p \quad \text{subject to} \quad \mathbf{w}_p^H \Upsilon_{p,t} \mathbf{w}_p = 1. \quad (32)$$

This problem is a complex-valued homogeneous QCQP, which is nonconvex because of the quadratic constraint. We use the SDR to reformulate (32) as

$$\begin{aligned} & \underset{\mathbf{W}_p}{\text{minimize}} \quad \text{Tr}(\tilde{\Upsilon}_c \mathbf{W}_p) \\ & \text{subject to} \quad \text{Tr}(\Upsilon_{p,t} \mathbf{W}_p) = 1, \mathbf{W}_p \succeq \mathbf{0}. \end{aligned} \quad (33)$$

Note that for a complex-valued homogeneous QCQP with three constraints or less, SDR is tight [66]. Denote the optimal solution of complex-value SDR (33) by \mathbf{W}_p^* , there always exists $\text{rank}(\mathbf{W}_p^*) \leq \sqrt{n_p}$ where n_p denotes the number of constraint [67]. This inequality leads to $\text{rank}(\mathbf{W}_p^*) = 1$ in problem (33). Hence, the optimal solution of problem (32) is obtained via eigenvalue decomposition (EVD) as $\mathbf{W}_p^* = \mathbf{w}_p^* \mathbf{w}_p^{*H}$. Note that (32) can also be solved using the Karush–Kuhn–Tucker (KKT) conditions or even successive convex approximation where the constraint is linearized via the first order Taylor approximation. In our numerical experiments, we empirically observe that the current SDR approach is already efficient.

B. Transmit beamformer design

Expanding the SINR expressions in (21) and (28), the square terms in the numerators and denominators yield inner products. We substitute the following expressions

$$\begin{aligned} \Xi_{p,c,k} &= \mathbf{I}_U \otimes (\tilde{\mathbf{A}}_{\text{dir},k} + \tilde{\mathbf{A}}_{\text{ind},k}(\Phi))^H \mathbf{w}_p \mathbf{w}_p^H (\tilde{\mathbf{A}}_{\text{dir},k} + \tilde{\mathbf{A}}_{\text{ind},k}(\Phi)), \\ & \quad (34a) \end{aligned}$$

$$\begin{aligned} \Xi_{p,t,k} &= \mathbf{I}_U \otimes (\mathbf{A}_{\text{dir},k,p} + \mathbf{A}_{\text{ind},k,p}(\Phi))^H \mathbf{w}_p \mathbf{w}_p^H (\mathbf{A}_{\text{dir},k,p} + \mathbf{A}_{\text{ind},k,p}(\Phi)), \\ & \quad (34b) \end{aligned}$$

$$\mathbf{R}_{u,k} = \mathbf{\Lambda}_u \otimes (\mathbf{h}_{u,k}^T + \mathbf{z}_{u,k}(\Phi))^H (\mathbf{h}_{u,k}^T + \mathbf{z}_{u,k}(\Phi)), \quad (34c)$$

$$\tilde{\mathbf{R}}_{u,k} = \tilde{\mathbf{\Lambda}}_u \otimes (\mathbf{h}_{u,k}^T + \mathbf{z}_{u,k}(\Phi))^H (\mathbf{h}_{u,k}^T + \mathbf{z}_{u,k}(\Phi)), \quad (34d)$$

in both SINRs, where the Kronecker product follows from the matrix identities [68, eqs. (520)-(524)]. Now, the optimization problem to design transmit beamformers with fixed \mathbf{w}_p and Φ_m becomes

$$\begin{aligned} & \underset{\mathbf{f}_1, \dots, \mathbf{f}_K}{\text{maximize}} \quad \min_p \frac{\sum_{k=1}^K \mathbf{f}_k^H \Xi_{p,t,k} \mathbf{f}_k}{\sum_{k=1}^K \mathbf{f}_k^H \Xi_{p,c,k} \mathbf{f}_k + K\sigma_R^2 \mathbf{w}_p^H \mathbf{w}_p} \\ & \text{subject to} \quad \|\mathbf{f}_k\|_2^2 \leq \mathcal{P}_k, \forall k, \quad \frac{\sum_{k=1}^K \mathbf{f}_k^H \mathbf{R}_{u,k} \mathbf{f}_k}{\sum_{k=1}^K \mathbf{f}_k^H \tilde{\mathbf{R}}_{u,k} \mathbf{f}_k + K\sigma_C^2} \geq \xi, \forall u, \end{aligned} \quad (35)$$

where $\mathbf{f}_k = \text{vec}(\mathbf{F}_k)$, $k = 1, \dots, K$. Next, we replace the summations in (34) by defining the following block diagonal matrices

$$\begin{aligned} \Xi_{p,t} &= \text{blkdiag}(\Xi_{p,t,1}, \dots, \Xi_{p,t,K}), \quad \Xi_{p,c} = \text{blkdiag}(\Xi_{p,c,1}, \dots, \Xi_{p,c,K}), \\ \mathbf{R}_u &= \text{blkdiag}(\mathbf{R}_{u,1}, \dots, \mathbf{R}_{u,K}), \quad \tilde{\mathbf{R}}_u = \text{blkdiag}(\tilde{\mathbf{R}}_{u,1}, \dots, \tilde{\mathbf{R}}_{u,K}). \end{aligned} \quad (36)$$

According to (36), the problem in (35) is equivalent to

$$\begin{aligned} & \underset{\mathbf{f} \in \mathbb{C}^{KN_t U \times 1}}{\text{maximize}} \quad \min_p \frac{\mathbf{f}^H \Xi_{p,t} \mathbf{f}}{\mathbf{f}^H \Xi_{p,c} \mathbf{f} + K\sigma_R^2 \mathbf{w}_p^H \mathbf{w}_p} \\ & \text{subject to} \quad \|\mathbf{V}_k \mathbf{f}\|_2^2 \leq \mathcal{P}_k, \forall k, \quad \frac{\mathbf{f}^H \mathbf{R}_u \mathbf{f}}{\mathbf{f}^H \tilde{\mathbf{R}}_u \mathbf{f} + K\sigma_C^2} \geq \xi, \forall u, \end{aligned} \quad (37)$$

where $\mathbf{f} = [\mathbf{f}_1^T, \dots, \mathbf{f}_K^T]^T$, \mathbf{V}_k denotes the selection matrix to extract k -th interval of \mathbf{f} , e.g., the vector \mathbf{f}_k . To tackle the maximin problem

(37), recall the following lemma about the generalized fractional programming (GFP), which states the requirement and method to achieve the optimal solution.

Lemma 1. [63] Consider two sets $\{g_p(\mathbf{x})\}_{p=1}^P$ and $\{f_p(\mathbf{x})\}_{p=1}^P$ of, respectively, convex and non-negative concave functions over a convex set \mathcal{X} . Then, the GFP problem

$$\underset{\mathbf{x}}{\text{maximize}} \quad \min_p \frac{f_p(\mathbf{x})}{g_p(\mathbf{x})} \quad \text{subject to} \quad \mathbf{x} \in \mathcal{X}, \quad (38)$$

is solvable and the optimal solution can be obtained via generalized Dinkelbach algorithm.

It follows from Lemma 1 that the generalized Dinkelbach algorithm is unable to solve the problem (37) because of the convexity of the numerator in the objective function and the second DC constraint. We aim to linearize these expressions through the following Lemma 2,

Lemma 2. For the function $f(\mathbf{x}) = \mathbf{x}^H \mathbf{H} \mathbf{x}$, the following inequality is always satisfied

$$f(\mathbf{x}) \geq 2\Re(\mathbf{x}^{(n)H} \mathbf{H} \mathbf{x}) - f(\mathbf{x}^{(n)}), \quad (39)$$

where \mathbf{H} is positive semidefinite (PSD) matrix, $\mathbf{x}^{(n)}$ denotes the current point (at the n -th iteration), and the equality holds if and only if $\mathbf{x} = \mathbf{x}^{(n)}$.

Proof: Define a real-valued function

$$g(\mathbf{x}_r) = \mathbf{x}_r^T \mathbf{H}_r \mathbf{x}_r, \quad (40)$$

where

$$\mathbf{x}_r = \begin{bmatrix} \Re\{\mathbf{x}\} \\ \Im\{\mathbf{x}\} \end{bmatrix}, \quad \mathbf{H}_r = \begin{bmatrix} \Re\{\mathbf{H}\} & -\Im\{\mathbf{H}\} \\ \Im\{\mathbf{H}\} & \Re\{\mathbf{H}\} \end{bmatrix}. \quad (41)$$

Observe that $f(\mathbf{x}) = g(\mathbf{x}_r)$ and $\mathbf{H}_r = \mathbf{H}_r^T$. Then,

$$\begin{aligned} g(\mathbf{x}_r) &\geq g(\mathbf{x}_r^{(n)}) + \nabla^T g(\mathbf{x}_r^{(n)})(\mathbf{x}_r - \mathbf{x}_r^{(n)}) \\ &= \mathbf{x}_r^{(n)T} \mathbf{H}_r \mathbf{x}_r^{(n)} + \mathbf{x}_r^{(n)T} (\mathbf{H}_r + \mathbf{H}_r^T)(\mathbf{x}_r - \mathbf{x}_r^{(n)}) \\ &= 2\mathbf{x}_r^{(n)T} \mathbf{H}_r \mathbf{x}_r - \mathbf{x}_r^{(n)T} \mathbf{H}_r \mathbf{x}_r^{(n)} \\ &= 2\Re(\mathbf{x}^{(n)H} \mathbf{H} \mathbf{x}) - g(\mathbf{x}_r^{(n)}) \\ &= 2\Re(\mathbf{x}^{(n)H} \mathbf{H} \mathbf{x}) - f(\mathbf{x}^{(n)}), \end{aligned} \quad (42)$$

where $\mathbf{x}_r^{(n)}$ is similarly defined as (41). From (40) and (42), we conclude that the inequality (39) always holds. This completes the proof. \blacksquare

Following Lemma 2, we reformulate the problem (37) and relax it by linearizing the numerator and communications SINR constraint as

$$\begin{aligned} & \underset{\mathbf{f}}{\text{maximize}} \quad \min_p \frac{2\Re(\mathbf{f}^{(n)H} \Xi_{p,t} \mathbf{f}) - \mathbf{f}^{(n)H} \Xi_{p,t} \mathbf{f}^{(n)}}{\mathbf{f}^H \Xi_{p,c} \mathbf{f} + K\sigma_R^2 \mathbf{w}_p^H \mathbf{w}_p} \\ & \text{subject to} \quad \|\mathbf{V}_k \mathbf{f}\|_2^2 \leq \mathcal{P}_k, \forall k, \\ & \quad \xi \mathbf{f}^H \tilde{\mathbf{R}}_u \mathbf{f} - 2\Re(\mathbf{f}^{(n)H} \mathbf{R}_u \mathbf{f}) \leq \text{const.}, \forall u \end{aligned} \quad (43)$$

where $\text{const.} = -\xi K\sigma_C^2 - \mathbf{f}^{(n)H} \mathbf{R}_u \mathbf{f}^{(n)}$ and n denotes the number of outer iteration. Note that the objective value of (37) is always greater than or equal to (43). Hence, solving (43) results in approximately solving (37). Now, problem (43) satisfies the requirements of GFP as in (38). Thus, we can solve problem (43) by reformulating it as

$$\begin{aligned} & \underset{\mathbf{f}}{\text{maximize}} \quad \min_p 2\Re(\mathbf{f}^{(n)H} \Xi_{p,t} \mathbf{f}) - \lambda_f \mathbf{f}^H \Xi_{p,c} \mathbf{f} \\ & \text{subject to} \quad \|\mathbf{V}_k \mathbf{f}\|_2^2 \leq \mathcal{P}_k, \forall k, \\ & \quad \xi \mathbf{f}^H \tilde{\mathbf{R}}_u \mathbf{f} - 2\Re(\mathbf{f}^{(n)H} \mathbf{R}_u \mathbf{f}) \leq \text{const.}, \forall u. \end{aligned} \quad (44)$$

Algorithm 1 Dinkelbach-based algorithm to solve (43)

Input: ζ_1 , $\mathbf{f}^{(n)}$, \mathcal{P}_k , \mathbf{R}_u , $\tilde{\mathbf{R}}_u$, $\tilde{\Xi}_{p,t}$, and $\tilde{\Xi}_{p,c}$.
Output: $\mathbf{f}^{(n)}$

- 1: Set $t_1 = 0$, $\mathbf{f}_{t_1} = \mathbf{f}^{(n)}$;
- 2: $\lambda_f^{(t_1)} = \min_p \frac{2\Re(\mathbf{f}^{(n)H} \tilde{\Xi}_{p,t} \mathbf{f}) - \mathbf{f}^{(n)H} \tilde{\Xi}_{p,t} \mathbf{f}^{(n)}}{\mathbf{f}^H \tilde{\Xi}_{p,c} \mathbf{f} + K \sigma_R^2 \mathbf{w}_p^H \mathbf{w}_p}$
- 3: **repeat**
- 4: Find \mathbf{f}_{t_1} by solving problem (44) using \mathcal{P}_k , \mathbf{R}_u , $\tilde{\mathbf{R}}_u$, $\tilde{\Xi}_{p,t}$, and $\tilde{\Xi}_{p,c}$;
- 5: $F_{\lambda_{t_1}} = \min_p 2\Re(\mathbf{f}^{(n)H} \tilde{\Xi}_{p,t} \mathbf{f}_{t_1}) - \lambda_f^{(t_1)} \mathbf{f}_{t_1}^H \tilde{\Xi}_{p,c} \mathbf{f}_{t_1}$;
- 6: $t_1 \leftarrow t_1 + 1$;
- 7: Update $\lambda_f^{(t_1)} = \min_p \frac{2\Re(\mathbf{f}^{(n)H} \tilde{\Xi}_{p,t} \mathbf{f}_{t_1}) - \mathbf{f}^{(n)H} \tilde{\Xi}_{p,t} \mathbf{f}^{(n)}}{\mathbf{f}_{t_1}^H \tilde{\Xi}_{p,c} \mathbf{f}_{t_1} + K \sigma_R^2 \mathbf{w}_p^H \mathbf{w}_p}$;
- 8: **until** $F_{\lambda_{t_1}} \leq \zeta_1$ or reach the maximum iteration. ;
- 9: **return** $\mathbf{f}^{(n)} = \mathbf{f}_{t_1}$;

The equivalent reformulation of this problem is by the epigraph form, which is then solved efficiently. Algorithm 1 summarizes this Dinkelbach-based method.

C. IRS phase-shifts design

With fixed \mathbf{w}_p and \mathbf{F}_k , the optimization problem to obtain IRS $_K$ phase-shifts is

$$\begin{aligned} & \underset{\Phi_m}{\text{maximize}} \quad \min_p \frac{\sum_{k=1}^K \|\mathbf{w}_p^H (\mathbf{A}_{p,\text{dir},k} + \mathbf{A}_{p,\text{ind},k}(\Phi)) \mathbf{F}_k\|_2^2}{\sum_{k=1}^K \|\mathbf{w}_p^H (\tilde{\mathbf{A}}_{\text{dir},k} + \tilde{\mathbf{A}}_{\text{ind},k}(\Phi)) \mathbf{F}_k\|_2^2 + K \sigma_R^2 \mathbf{w}_p^H \mathbf{w}_p} \\ & \text{subject to} \quad \text{SINR}_{C_u} \geq \xi, \forall u, |\Phi(i, i)| = 1, \forall i. \end{aligned} \quad (45)$$

It is very challenging to directly solve this problem because of the fractional quartic objective function, DC, and constant modulus constraints. Define the vector $\phi = [\phi_1^T, \dots, \phi_M^T]^T$, where $\phi_m = \Phi_m \mathbf{1}_{N_m}$. The cascaded communications channel matrices of u -th user is $\mathbf{H}_{u,k} = [\text{diag}(\mathbf{h}_{u,1,k}) \mathbf{G}_{1,k}, \dots, \text{diag}(\mathbf{h}_{u,M,k}) \mathbf{G}_{M,k}]^T$, and $q_u = \sum_{k=1}^K \mathbf{h}_{u,k}^T \mathbf{F}_k \Lambda_u \mathbf{F}_k^H \mathbf{h}_{u,k}^*$, $\bar{q}_u = \sum_{k=1}^K \mathbf{h}_{u,k}^T \mathbf{F}_k \bar{\Lambda}_u \mathbf{F}_k^H \mathbf{h}_{u,k}^*$, $\mathbf{q}_u = \sum_{k=1}^K \mathbf{H}_{u,k}^* \mathbf{F}_k^* \Lambda_u \mathbf{F}_k^T \mathbf{h}_{u,k}$, $\bar{\mathbf{q}}_u = \sum_{k=1}^K \mathbf{H}_{u,k}^* \mathbf{F}_k^* \bar{\Lambda}_u \mathbf{F}_k^T \mathbf{h}_{u,k}$, $\mathbf{Q}_u = \sum_{k=1}^K \mathbf{H}_{u,k}^* \mathbf{F}_k^* \Lambda_u \mathbf{F}_k^T \mathbf{H}_{u,k}$, and $\bar{\mathbf{Q}}_u = \sum_{k=1}^K \mathbf{H}_{u,k}^* \mathbf{F}_k^* \bar{\Lambda}_u \mathbf{F}_k^T \mathbf{H}_{u,k}$. Then, we introduce the auxiliary variables $\psi = \phi$ to convert problem (45) into the bi-fractional quadratic programming as

$$\begin{aligned} & \underset{\phi, \psi}{\text{maximize}} \quad \min_p \frac{\bar{f}_p(\phi, \psi)}{\bar{g}_p(\phi, \psi)} \\ & \text{subject to} \quad \phi = \psi, |\phi(i)| = 1, |\psi(i)| = 1, \forall i \\ & \quad \frac{q_u + 2\Re\{\phi^H \mathbf{q}_u\} + \phi^H \mathbf{Q}_u \phi}{\bar{q}_u + 2\Re\{\phi^H \bar{\mathbf{q}}_u\} + \phi^H \bar{\mathbf{Q}}_u \phi + K \sigma_C^2} \geq \xi, \forall u, \end{aligned} \quad (46)$$

Rewrite the objective function as

$$\begin{aligned} \bar{f}_p(\phi, \psi) &= \phi^H \mathbf{U}_p \phi + 2\Re(\phi^H \mathbf{u}_p) + u_p = \psi^H \mathbf{V}_p \psi + 2\Re(\phi^H \mathbf{v}_p) + v_p, \\ \bar{g}_p(\phi, \psi) &= \phi^H \tilde{\mathbf{U}}_p \phi + 2\Re(\phi^H \tilde{\mathbf{u}}_p) + \tilde{u}_p = \psi^H \tilde{\mathbf{V}}_p \psi + 2\Re(\phi^H \tilde{\mathbf{v}}_p) + \tilde{v}_p. \end{aligned} \quad (47)$$

where

$$\begin{aligned} \mathbf{U}_{k,p} &= \begin{bmatrix} \text{diag}(\mathbf{w}_p^H \mathbf{E}_{1,k,p}) \mathbf{G}_{1,k} + \text{diag}(\mathbf{w}_p^H \mathbf{D}_{1,k}) \mathbf{B}_{1,k,p} + \text{diag}(\mathbf{w}_p^H \mathbf{D}_{1,k}) \mathbf{W}_{1,k,p} \psi_1 \mathbf{G}_{1,k} \\ \vdots \\ \text{diag}(\mathbf{w}_p^H \mathbf{E}_{m,k,p}) \mathbf{G}_{m,k} + \text{diag}(\mathbf{w}_p^H \mathbf{D}_{m,k}) \mathbf{B}_{m,k,p} + \text{diag}(\mathbf{w}_p^H \mathbf{D}_{m,k}) \mathbf{W}_{m,k,p} \psi_m \mathbf{G}_{m,k} \end{bmatrix}, \\ u_p &= \sum_{k=1}^K \mathbf{w}_p^H \mathbf{A}_{p,\text{dir},k} \mathbf{F}_k \mathbf{F}_k^H \mathbf{A}_{p,\text{dir},k}^H \mathbf{w}_p, \\ \mathbf{u}_p &= \sum_{k=1}^K \mathbf{U}_{k,p}^* \mathbf{F}_k^* \mathbf{F}_k^T \mathbf{A}_{p,\text{dir},k}^T \mathbf{w}_p^*, \\ \mathbf{U}_p &= \sum_{k=1}^K \mathbf{U}_{k,p}^* \mathbf{F}_k^* \mathbf{F}_k^T \mathbf{U}_{k,p}^T, \\ \mathbf{V}_{k,p} &= \begin{bmatrix} \text{diag}(\mathbf{w}_p^H \mathbf{D}_{1,k} \Phi_1 \mathbf{W}_{1,k,p}) \mathbf{G}_{1,k} \\ \vdots \\ \text{diag}(\mathbf{w}_p^H \mathbf{D}_{m,k} \Phi_m \mathbf{W}_{m,k,p}) \mathbf{G}_{m,k} \end{bmatrix}, \\ \mathbf{V}_p &= \sum_{k=1}^K \mathbf{V}_{k,p}^* \mathbf{F}_k^* \mathbf{F}_k^T \mathbf{V}_{k,p}^T, \\ \mathbf{v}_p &= \sum_{k=1}^K \mathbf{V}_{k,p}^* \mathbf{F}_k^* \mathbf{F}_k^T (\mathbf{A}_{k,p}^T \\ & \quad + \sum_{m=1}^M (\mathbf{G}_{m,k}^T \Phi_m^T \mathbf{E}_{m,k,p}^T + \mathbf{B}_{m,k,p}^T \Phi_m^T \mathbf{D}_{m,k}^T)) \mathbf{w}_p^*, \\ v_p &= \sum_{k=1}^K \left\| \mathbf{w}_p^H \mathbf{A}_{p,\text{dir},k} \mathbf{F}_k + \sum_{m=1}^M \mathbf{w}_p^H (\mathbf{E}_{m,k,p} \Phi_m \mathbf{G}_{m,k} + \mathbf{D}_{m,k} \Phi_m \mathbf{B}_{m,k,p}) \mathbf{F}_k \right\|^2. \end{aligned} \quad (48)$$

Similarly, $\tilde{\mathbf{U}}_p$, $\tilde{\mathbf{V}}_p$, $\tilde{\mathbf{u}}_p$, $\tilde{\mathbf{v}}_p$, \tilde{u}_p , and \tilde{v}_p are also analogously defined by replacing $\mathbf{A}_{\text{dir},k}$, $\mathbf{E}_{m,k,p}$, $\mathbf{B}_{m,k,p}$, and $\mathbf{W}_{m,k,p}$ with $\tilde{\mathbf{A}}_{\text{dir},k}$, $\tilde{\mathbf{E}}_{m,k,p}$, $\tilde{\mathbf{B}}_{m,k,p}$, and $\tilde{\mathbf{W}}_{m,k,p}$, respectively.

Following Dinkelbach framework, (46) becomes

$$\begin{aligned} & \underset{\phi, \psi}{\text{maximize}} \quad \min_p \bar{f}_p(\phi, \psi) - \lambda_\phi \bar{g}_p(\phi, \psi) \\ & \text{subject to} \quad \phi = \psi, |\phi(i)| = 1, |\psi(i)| = 1, \forall i, \\ & \quad \frac{q_u + 2\Re\{\phi^H \mathbf{q}_u\} + \phi^H \mathbf{Q}_u \phi}{\bar{q}_u + 2\Re\{\phi^H \bar{\mathbf{q}}_u\} + \phi^H \bar{\mathbf{Q}}_u \phi + K \sigma_C^2} \geq \xi, \forall u. \end{aligned} \quad (49)$$

where λ_ϕ denotes the Dinkelbach parameter. Convert (49) to the equivalent

$$\begin{aligned} & \underset{\phi, \psi}{\text{minimize}} \quad \max_\omega \sum_{p=1}^P \omega_p (\lambda_\phi \bar{g}_p(\phi, \psi) - \bar{f}_p(\phi, \psi)) \\ & \text{subject to} \quad \phi = \psi, |\phi(i)| = 1, |\psi(i)| = 1, \forall i \\ & \quad \frac{q_u + 2\Re\{\phi^H \mathbf{q}_u\} + \phi^H \mathbf{Q}_u \phi}{\bar{q}_u + 2\Re\{\phi^H \bar{\mathbf{q}}_u\} + \phi^H \bar{\mathbf{Q}}_u \phi + K \sigma_C^2} \geq \xi, \forall u, \end{aligned} \quad (50)$$

where $\omega \succeq \mathbf{0}$ and $\|\omega\|_1 = 1$.

From [69] and Lemma 2, we further linearize the communications SINR in (37) as

$$2\Re\{\mathbf{r}_u^H \phi\} \leq d_u, \forall u, \quad (51)$$

where $\mathbf{r}_u = (\xi \phi_t^H (\bar{\mathbf{Q}}_u - \eta_u \mathbf{I}) + \xi \bar{\mathbf{q}}_u^H - \mathbf{q}_u^H - \phi_t^H \mathbf{Q}_u)^H$, η_u is the largest eigenvalue of $\bar{\mathbf{Q}}_u$, $d_u = \xi(\bar{q}_u + K \sigma_C^2 - 2\eta_u M N_m + \phi_t^H \bar{\mathbf{Q}}_u \phi_t) + \phi_t^H \mathbf{Q}_u \phi_t - q_u$, and ϕ_t denotes the value of ϕ at t -th iteration. If the inequality (51) holds, the original SINR inequality constraint is always satisfied. The augmented Lagrangian function of (50) is

$$\mathcal{L}(\phi, \psi, \mathbf{u}, \mathbf{w}, \rho) = f(\phi, \psi, \lambda_\phi) + \frac{\rho}{2} \|\phi - \psi + \mathbf{u}\|_2^2 + \Re\{\mathbf{w}^T \mathbf{c}\} \quad (52)$$

where $f(\phi, \psi, \lambda_\phi) = \max_\omega \sum_{p=1}^P \omega_p (\lambda_\phi \bar{g}_p(\phi, \psi) - \bar{f}_p(\phi, \psi))$, $\mathbf{c} = [c_1, \dots, c_U]^T$, $c_u = 2\Re\{\mathbf{r}_u^H \phi\} - d_u$, ρ is the penalty parameter,

Algorithm 2 C-ADMM algorithm to solve (50)

Input: $\zeta_2, \mathbf{u}, \mathbf{w}, \psi^{(n)}$ and $\phi^{(n)}$
Output: $\phi^{(n)*} = \phi_{t_2}$.

- 1: Set $t_2 = 0$;
- 2: **repeat**
- 3: Compute: $\lambda_\phi^{(t_2)} = \min_p \frac{\bar{f}_p(\phi^{(n)}, \psi^{(n)})}{\bar{g}_p(\phi^{(n)}, \psi^{(n)})}$;
- 4: Update ϕ_{t_2} via solving

$$\text{minimize}_{\phi^{(n)}} \mathcal{L}(\phi^{(n)}, \psi^{(n)}, \mathbf{u}, \mathbf{w}, \rho) \quad \text{subject to } |\phi^{(n)}| = 1. \quad (53)$$
- 5: Update ψ_{t_2} via solving

$$\text{minimize}_{\psi^{(n)}} \mathcal{L}(\phi^{(n)}, \psi^{(n)}, \mathbf{u}, \mathbf{w}, \rho) \quad \text{subject to } |\psi^{(n)}| = 1. \quad (54)$$
- 6: Update the dual variable \mathbf{u} and \mathbf{w} ;
- 7: $t_2 \leftarrow t_2 + 1$;
- 8: **until** $\|\phi_{t_2} - \phi_{t_2-1}\|_2^2 \leq \zeta_2$ or reach the maximum iteration;
- 9: **return** ϕ_{t_2} ;

Algorithm 3 RSD algorithm for manifold optimization

Input: $\lambda_\phi^{(t_2)}, \mathbf{u}, \mathbf{w}, \psi^{(n)}$ and $\phi^{(n)}$.
Output: $\phi_{t_2} = \phi_{t_3}$.

- 1: Set $t_3 = 0, \phi_{t_3} = \phi_n$;
- 2: **repeat**
- 3: Calculate ω by solving (57) with fixed ϕ_{t_3} ;
- 4: Linearize the function $\bar{f}_p(\phi, \psi)$ using (56) and $\phi^{(n)}$;
- 5: Compute Euclidean gradient $\nabla \mathcal{L}(\phi_{t_3})$ as (58) using \mathbf{u}, \mathbf{w} and $\psi^{(n)}$;
- 6: Compute Riemannian gradient as $\text{grad} \mathcal{L}(\phi_{t_3})$ as (59);
- 7: Update ϕ_{t_3} via the retraction procedure as (60);
- 8: $\lambda_\phi^{(t_3)} \leftarrow \min_p \frac{\bar{f}_p(\phi, \psi)}{\bar{g}_p(\phi, \psi)}$;
- 9: $t_3 \leftarrow t_3 + 1$;
- 10: **until** $\lambda_\phi^{(t_3)} \geq \lambda_\phi^{(t_2)}$ or maximum iteration reached;
- 11: **return** ϕ_{t_3} ;

\mathbf{u} and $\mathbf{w} \succeq \mathbf{0}$ denote the auxiliary variables. Based on above, we summarize our C-ADMM algorithm for solving (50) in Algorithm 2.

Based on above, the subproblem in Step 4 of Algorithm 2 becomes

$$\text{minimize}_{\phi} \max_{\omega} \sum_{p=1}^P \omega_p (\lambda_\phi \bar{g}_p(\phi, \psi) - \bar{f}_p(\phi, \psi)) + \frac{\rho}{2} \|\phi - \psi + \mathbf{u}\|_2^2 + \Re\{\mathbf{w}^T \phi\} \quad (55)$$

subject to $|\phi| = 1$.

It is still difficult to apply the RSD algorithm to solve problem (55) because of the concave function $\bar{f}_p(\phi, \psi)$ in the objective. We utilize Lemma 2 to linearize it as

$$\bar{f}_p(\phi, \psi) \geq 2\Re\{\phi^H (\mathbf{U}_p \phi^{(n)} + \mathbf{u}_p)\} + \phi^{(n)H} \mathbf{U}_p \phi^{(n)} + \mathbf{u}_p. \quad (56)$$

Substituting $\bar{f}_p(\phi, \psi)$ by its lower bound in (52), problem (51) becomes

$$\text{minimize}_{\phi} \max_{\omega} \sum_{p=1}^P \omega_p (\lambda_\phi \bar{g}_p(\phi, \psi) - 2\Re\{\phi^H (\mathbf{U}_p \phi^{(n)} + \mathbf{u}_p)\}) + \frac{\rho}{2} \|\phi - \psi + \mathbf{u}\|_2^2 + \Re\{\mathbf{w}^T \mathbf{c}\} \quad (57)$$

subject to $|\phi| = 1$.

It follows that problem (57) is the manifold optimization problem, which is solved by the RSD algorithm [35]. In order to obtain the

Algorithm 4 Alternating maximization algorithm to solve (29)

Input: $\zeta_3, \mathbf{w}_p^{(n)}, \mathbf{f}^{(n)}$, and $\phi^{(n)}$.
Output: $\mathbf{w}_p^* = \mathbf{w}_p^{(n)}, \mathbf{F}_k^* = \mathbf{F}_k^{(n)}$ and $\phi_m^* = \phi_m^{(n)}$.

- 1: Set $n = 0$;
- 2: **repeat**
- 3: Update $\mathbf{W}_p^{(n)}, p = 1, \dots, P$ via solving problem (33);
- 4: Update $\mathbf{w}_p^{(n)}$ as the principle eigenvector of $\mathbf{W}_p^{(n)}$;
- 5: Update $\mathbf{f}^{(n)}$ via **Algorithm 1**, and reconstruct $\mathbf{F}_k^{(n)}, k = 1, \dots, K$ via $\mathbf{f}^{(n)}$;
- 6: Update $\phi^{(n)}$ via **Algorithms 2 and 3**;
- 7: Reconstruct $\phi_m^{(n)}, m = 1, \dots, M$ via $\phi^{(n)}$;
- 8: $n \leftarrow n + 1$;
- 9: **until** $\|\mathbf{f}^{(n)} - \mathbf{f}^{(n-1)}\|_2^2 \leq \zeta_3$ or maximum iterations reached;
- 10: **return** $\mathbf{w}_p^{(n)}, \mathbf{F}_k^{(n)}$, and $\phi_m^{(n)}$;

Riemannian gradient, we first calculate the Euclidean gradient of the objective function in (57) as

$$\begin{aligned} \nabla \mathcal{L}(\phi) = & \lambda_\phi (2\tilde{\mathbf{U}}_p \phi + 2\tilde{\mathbf{u}}_p) - 2(\mathbf{U}_p \phi^{(n)} + \mathbf{U}_p) + \rho(\phi - \psi - \mathbf{u}) \\ & + \sum_{u=1}^U w_u (2\tilde{\mathbf{Q}}_u \phi + 2\tilde{\mathbf{q}}_u). \end{aligned} \quad (58)$$

Then, the Riemannian gradient is obtained by projecting $\nabla \mathcal{L}(\phi)$ into the tangent space as

$$\text{grad} \mathcal{L}(\phi) = \nabla \mathcal{L}(\phi) - \Re\{\nabla \mathcal{L}(\phi) \odot \phi\} \odot \phi. \quad (59)$$

Now, we update it by retracting ϕ into the complex circle manifold as

$$\phi = \frac{\phi - \alpha \text{grad} \mathcal{L}(\phi)}{|\phi - \alpha \text{grad} \mathcal{L}(\phi)|}. \quad (60)$$

In each C-ADMM iteration, the subproblem related with ϕ is solved by Algorithm 3.

Similarly, the subproblem in Step 4 of Algorithm 2 is

$$\begin{aligned} \text{minimize}_{\psi} \max_{\omega} \sum_{p=1}^P \omega_p (\lambda_\phi \bar{g}_p(\phi, \psi) - \bar{f}_p(\phi, \psi)) + \frac{\rho}{2} \|\phi - \psi + \mathbf{u}\|_2^2 \\ \text{subject to } |\psi| = 1, \end{aligned} \quad (61)$$

which is also solved via Algorithm 3 with the change of the optimization variable.

To summarize, we utilize SDR for the receive filter bank design. Then, the Dinkelbach-based method yields the transmit beamformers. Finally, the C-ADMM updates the phase-shifts Φ_m . Based on above discussion, the overall AM-based procedure is summarized in Algorithm 4.

D. Computational complexity

The overall computational burden of Algorithm 4 is linear with the number of outer iterations. Meanwhile, at each outer iteration, the closed-form solution of Doppler filter $\mathbf{w}_p, p = 1, \dots, P$ is given by solving problem (33) with the complexity of $\mathcal{O}(PN_r^{3.5})$. Then, to update the transmit beamforming matrix $\mathbf{F}_k, k = 1, \dots, K$, the computational cost of Algorithm 1 is linear with the number of inner iterations T_1 . At each inner iteration of the Dinkelbach-based method, problem (44) is solved by the CVX [70] with the complexity of $\mathcal{O}(K^3 N_t^3 U^3)$. In order to update the phase-shift matrix $\Phi_m, m = 1, \dots, M$, the C-ADMM and RSD algorithm are combined with the total complexity $\mathcal{O}(T_2(2T_3 M^2 N_m^2 + M^2 N_m^2))$, where T_2 and T_3 denote the maximum iteration number of C-ADMM and RSD,

respectively. Finally, the total complexity of the proposed algorithm is $\mathcal{O}(PN_r^{3.5} + T_1 K^3 N_t^3 U^3 + T_2(2T_3 M^2 N_m^2 + M^2 N_m^2))$ for each outer iteration.

IV. NUMERICAL EXPERIMENTS

Unless otherwise specified, throughout all experiments, the dual-function transmitter and radar receiver are equipped with a ULA comprising $N_t = 6$ and $N_r = 4$ elements, respectively. The location of DFBS is set to $\mathbf{p}_d = [0 \text{ m}, 0 \text{ m}]$. A single fast moving target is located at $\mathbf{p}_t = [0 \text{ m}, 5000 \text{ m}]$ with the speed $\mathbf{v} = [v_x, v_y]$, where the intervals $v_x \in (100 \text{ m/s}, 500 \text{ m/s}]$ and $v_y \in (10 \text{ m/s}, 50 \text{ m/s}]$ are uniformly divided into $P = 5$ discrete grid points. Two stationary clutter scatterers are located at 20° and -20° with respect to the DFBS. Two IRSs located at $\mathbf{p}_{i_1} = [2500\text{m}, 2500\text{m}]$ and $\mathbf{p}_{i_2} = [-2500\text{m}, 2500\text{m}]$ are deployed to assist the DFRC system. Each IRS consists of 20 reflecting elements. Meanwhile, the dual-function transmitter serves $U = 2$ single-antenna users.

The central frequency of the wideband DFRC is $f_c = 10 \text{ GHz}$ and the frequency step of OFDM is set to $\Delta f = 20 \text{ MHz}$. The total number of subcarriers is $K = 32$. The inter-element spacing for the transmitter, receiver, and IRS arrays is set to the half wavelength of the highest frequency, i.e., $d = c/2f_{max}$ and $f_{max} = 10.32 \text{ GHz}$ to reduce the grating lobes [58]. The transmit power at all subcarriers is set to $\mathcal{P}_1 = \dots, \mathcal{P}_K = 1 \text{ dBW}$. The noise variances are $\sigma_R^2 = 5 \text{ dB}$ and $\sigma_C^2 = -5 \text{ dB}$. We set the SINR threshold for all users to $\xi = 10 \text{ dB}$. The channel gain of direct paths are $\alpha_1 = 1$ and $\beta_1 = 1$ for target and clutter, respectively. The same for the indirect paths (i.e., IRS-aided channel) are $\alpha_{m,2} = \alpha_{m,3} = \alpha_{m,4} = 0.3$ and $\beta_2 = \beta_3 = \beta_4 = 0.3$ for target and clutter, respectively.

The Doppler receive filter $\mathbf{w}_p, p = 1 \dots, P$ and the transmit beamformers $\mathbf{F}_k, k = 1, \dots, K$ are randomly generated column vectors and matrices, whose entries follow zero-mean Gaussian distribution and satisfy $\|\mathbf{F}_k\|_F^2 \leq \mathcal{P}_k$. The phase-shift matrices $\Phi_m, m = 1 \dots, M$ are initialized with the diagonal entries generated from a complex value with unimodulus amplitude and random phase, i.e., $e^{j\phi_m}$, where $\phi_m \in (0, 2\pi]$. We calculate the radar detection probability and false alarm probability based on Monte Carlo simulations with $N_{mont} = 10^4$ iterations. For the CSI matrices $\mathbf{h}_{u,k}$ and $\mathbf{h}_{u,m,k}$ with $u = 1, \dots, U$, we assume α_l and $\alpha_{l,m} \sim \mathcal{CN}(0, 1)$, the number of clusters are set to $L = 15$ and $L_m = 15, \forall m$, the pulse shaping function $r(t)$ can be modeled as the raised-cosine filter [71], the paths delay τ_l and $\tau_{l,m}$ is uniformly distributed in $[0, KT_s]$ with $T_s = 1$, the AoDs of all clusters, i.e., ϕ_l and $\phi_{l,m}$, are randomly distributed in $(0, 2\pi]$.

The initial decent step-size for RSD algorithm is $\alpha = 10^{-6.5}$ and we use the parameter 0.1 to scale it with the increasing of each outer AM iteration. Finally, the maximum iteration number is set to $T_1 = 20, T_2 = 20$, and $T_3 = 100$ for Algorithm 1, Algorithm 2, and Algorithm 3, respectively. Meanwhile, the maximum iteration number for the overall Algorithm 4 is $N = 30$.

In order to evaluate the performance of radar detection, we first generate the receive signal $\tilde{\mathbf{y}}_{R_p}[f_k]$ in (20) with the transmit symbol $\mathbb{E}\{\mathbf{s}_k \mathbf{s}_k^H\} = \mathbf{I}$ and noise $\tilde{\mathbf{n}}_R[f_k] \in \mathcal{CN}(0, \sigma_R^2 \mathbf{I})$. Then, we transmit (20) to discrete-time domain using K -point IFFT and consider the following binary hypothesis problem

$$\begin{cases} \mathcal{H}_0: \mathbf{y}_{R_0}[\tilde{n}] = \mathbf{c}_{ind}[\tilde{n}] + \mathbf{c}_{ind}[\tilde{n}] + \mathbf{n}_R[\tilde{n}], \\ \mathcal{H}_1: \mathbf{y}_{R_p}[\tilde{n}] = \mathbf{s}_{dir_p}[\tilde{n}] + \mathbf{s}_{ind_p}[\tilde{n}] + \mathbf{c}_{dir}[\tilde{n}] + \mathbf{c}_{ind}[\tilde{n}] + \mathbf{n}_R[\tilde{n}], \end{cases} \quad (62)$$

where $\tilde{n} = 1, \dots, K$. We compute the empirical probabilities of detection P_D and false alarm P_{FA} in the post-Doppler-bank stage as follows.

Case 1: Under hypothesis \mathcal{H}_0 , the average power over all subcarriers is

$$\max_p \sum_{\tilde{n}=1}^K |\mathbf{w}_p^H \mathbf{y}_{R_0}[\tilde{n}]|^2 = \tilde{\beta}_0, \quad (63)$$

and, for a certain threshold γ ,

$$\begin{cases} \text{if } \tilde{\beta}_0 > \gamma, & \text{false alarm,} \\ \text{if } \tilde{\beta}_0 \leq \gamma, & \text{no false alarm.} \end{cases} \quad (64)$$

Based on above, we count the total number of false alarms N_{FA} to obtain $P_{FA} = \frac{N_{FA}}{N_{mont}}$.

Case 2: Under hypothesis \mathcal{H}_1 , we compute the average power over all subcarriers as

$$\max_p \sum_{\tilde{n}=1}^K |\mathbf{w}_p^H \mathbf{y}_{R_p}[\tilde{n}]|^2 = \tilde{\beta}_1, \quad (65)$$

and

$$\begin{cases} \text{if } \tilde{\beta}_1 > \gamma, & \text{detection,} \\ \text{if } \tilde{\beta}_1 \leq \gamma, & \text{no detection.} \end{cases} \quad (66)$$

Based on above, we count the total number of detection N_D to obtain $P_D = \frac{N_D}{N_{mont}}$. Throughout all experiments, we set the discrete value of threshold $\gamma \in [0, 10]$ with the step-size 0.1.

A. Convergence

The left plot of Fig. 2a illustrates the convergence of Dinkelbach-based algorithm to solving the subproblem related to transmit beamformer design in the first AM iteration. Note that even though the linearization step is utilized for both objective function and constraint, the proposed Dinkelbach-based algorithm is convergent in around 5 iterations. The objective value (i.e., minimum radar SINR) is monotonically increasing with the iterations because the objective value of the original problem (37) is always greater than the linearized problem (43) and Dinkelbach method can guarantee the monotonic objective value and hence the optimal solution. The right figure of Fig. 2a shows the convergence behavior of the RSD algorithm. The results shows that for the nonconvex manifold optimization problem, the RSD is convergent to the preferable value within 100 iterations with some fluctuation.

Fig. 2b demonstrates the convergence performance of proposed overall AM algorithm. We observe that it converges within 10 iterations. The non-IRS radar-only system has a better performance than a non-IRS DFRC because the latter needs to allocate a portion of transmit power to serve the users while the radar-only system utilizes all available power for target detection. If we use random phase-shifts for IRS, the radar SINR is lower than the one obtained after optimizing the phase-shifts but higher than the non-IRS case. Optimizing the phase-shifts leads to at least 3.5 and 13 dB radar SINR gain for single-IRS and multi-IRS deployments, respectively. Finally, the achievable minimum radar SINR for multi-IRS DFRC is higher than non-IRS DFRC, non-IRS radar-only and single-IRS DFRC system because of more overall reflecting elements and RCS diversity resulting from multi-IRS deployment.

B. Beam patterns

Fig. 3 compares the wideband transmit beam pattern for different scenarios. The non-IRS radar-only system exactly aligns the main beam toward the target direction and forms two nulls toward the clutter scatterers direction at all subcarriers. However, non-IRS DFRC system is unable to focus all transmit energy toward the target direction at all subcarriers because of the QoS requirement of communications users. Meanwhile, for single-IRS DFRC system, a

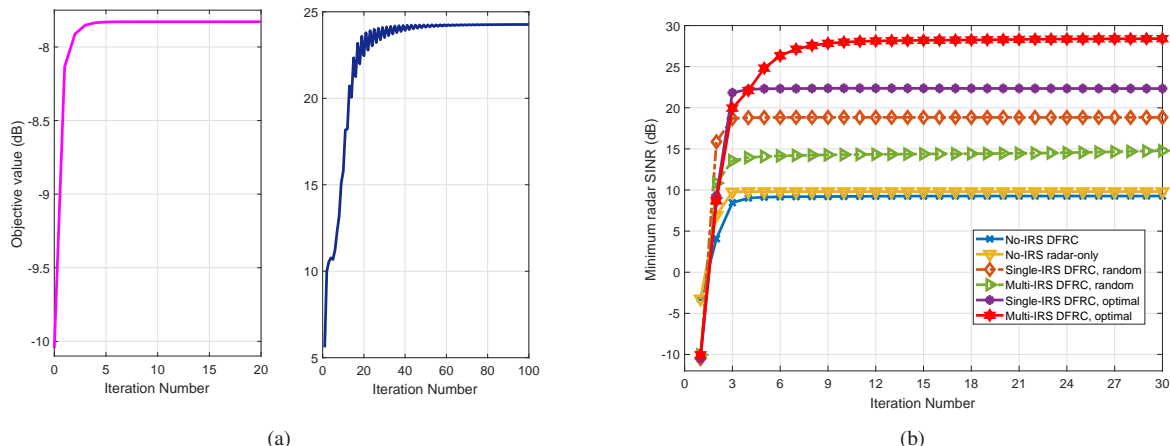


Fig. 2. Convergence behaviour of (a) left: Dinkelbach-based algorithm, right: RSD algorithm, and (b) the overall AM-based algorithm in terms of the minimum radar SINR as the number of iterations.

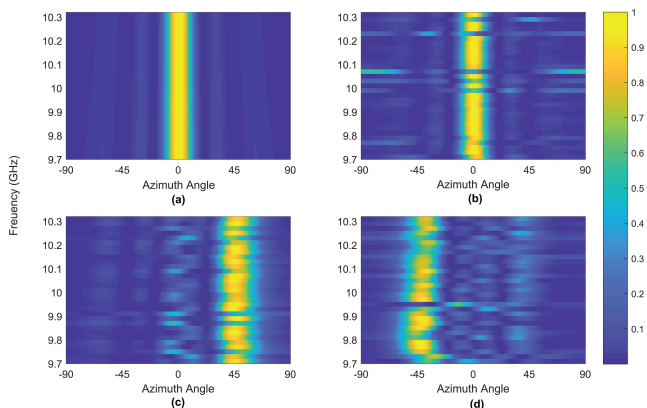


Fig. 3. The normalized spatial-frequency spectrum for different scenarios given $\theta_t = 0^\circ$, $\theta_{c_1} = 20^\circ$ and $\theta_{c_2} = -20^\circ$: (a) non-IRS radar system, (b) non-IRS DFRC system, (c) single-IRS DFRC system, $\theta_{i_1} = 45^\circ$, and (d) multi-IRS DFRC system with $\theta_{i_1} = 45^\circ$ and $\theta_{i_2} = -45^\circ$.

majority of transmit energy focuses toward the direction of IRS and the rest of it is directly aligned toward the target. This means the IRS-aided path is extensively used even with a lower channel gain compared with the direct path. For multi-IRS DFRC, the two IRSs are largely utilized for enhancing the overall system performance. Note that if the transmit power is increased, the beam for each subcarrier may get aligned toward the IRS direction more uniformly.

C. Radar performance

Fig. 4a demonstrates the achievable radar SINR at different Doppler slices. Unsurprisingly, it is seen that the proposed multi-IRS DFRC scheme achieves the highest radar SINR gain over all Doppler slices. Meanwhile, even though the initial SINR for each Doppler slice is dramatically different, we finally attain almost the same radar SINR at different Doppler slices. This shows the robustness of the proposed method against the unknown Doppler shift.

The receiver operating characteristic curve that plots P_D versus P_{FA} is shown in Fig. 4b. Here, the non-IRS radar-only and non-IRS DFRC systems achieve the nearly identical performance because both have a similar radar SINR after the beamformer design. With the same false alarm probability, e.g., 0.1, the proposed multi-IRS DFRC system achieves a higher detection probability compared with the non-IRS

and single-IRS cases, effectively highlighting the superiority of our proposed multi-IRS-aided DFRC system.

Fig. 5a demonstrates the minimum radar SINR versus the transmit power of each subcarriers. The increase in the transmit power obviously improves the minimum achievable radar SINR for all systems. The single-IRS DFRC with random phase-shifts has a better performance than the multi-IRS with random phase-shift because, if the phase-shifts are not optimized, multiple IRS deployments lead to massive interference from clutter scatterers often exceeding the signal gain from target. On the other side, the increase in transmit power narrows the gap between DFRC and radar-only system in the non-IRS case. Hence, given the certain communications SINR constraint, if the DFRC system needs to achieve the nearly same radar performance with radar-only system, the transmit power should be significantly boosted. Furthermore, the multi-IRS DFRC with the optimal phase-shift certainly provides the best radar SINR for different power settings because of the higher indirect path gain. Table II compares the performance of frequency-dependent and frequency-independent beamforming. The beam-squint effect implies that the frequency-independent narrowband beamformer has a lower radar SINR than the frequency-dependent wideband scheme for all systems. Hence, it is imperative to design digital beamformers for each subcarrier in a wideband system.

Fig. 5b plots the minimum radar SINR versus the communications SINR. Compared to the radar-only system, the increase in communications SINR leads to the performance loss for radar SINR; a higher communications SINR requirement exacerbates this loss. Hence, IRS-aided DFRC system requires a performance trade-off between radar and communications. Fig. 5c presents the minimum radar SINR versus the number of transmit antennas. As expected, the increase in transmit antennas improves the radar SINR. It yields at least 0.5 dB enhancement per transmit antenna. Similarly, more transmit antennas also narrow the performance gap between the non-IRS DFRC and non-IRS radar-only system.

Fig. 5d displays the minimum radar SINR with respect to the reflecting elements of IRS. It is interesting to note that the increase in the number of IRS elements brings the obvious improvement of radar SINR for the multi-IRS DFRC with the optimal phase-shift compared with the non-IRS and single-IRS cases. Meanwhile, for IRS-aided DFRC with random phase-shifts, an increase in reflecting elements may lead to a degradation of radar SINR, thereby directly underlining the importance of phase-shift optimization. Finally, in the optimal phase-shift multi-IRS DFRC, beyond a certain number

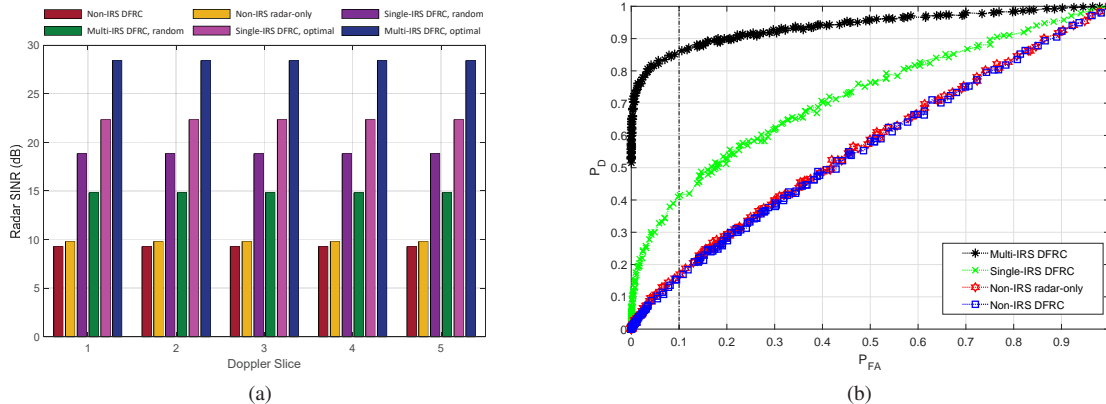


Fig. 4. (a) Minimum radar SINR versus Doppler slices, in which the Doppler range was discretized to 5 grid points. (b) Radar detection probability versus false alarm probability.

TABLE II
RADAR SINR FOR WIDEBAND AND NARROWBAND BEAMFORMING

Method	Narrowband	Wideband	Method	Narrowband	Wideband
Non-IRS DFRC	6.740 dB	9.268 dB	Multi-IRS DFRC, random	10.646 dB	14.777 dB
Non-IRS radar-only	7.105 dB	9.801 dB	Single-IRS DFRC, optimal	20.011 dB	22.336 dB
Single-IRS DFRC, random	12.054 dB	18.830 dB	Multi-IRS DFRC, optimal	22.025 dB	28.408 dB

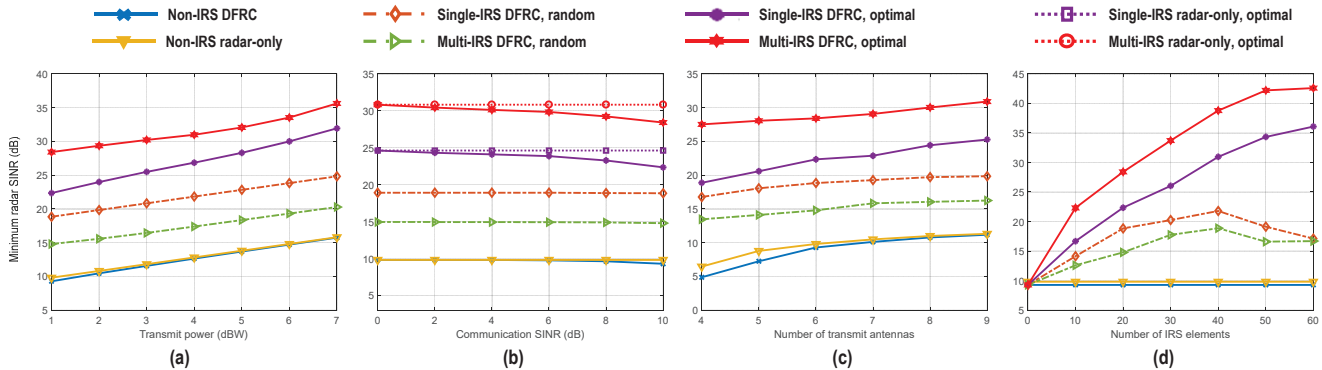


Fig. 5. Illustration of radar performance, (a) minimum radar SINR versus transmit power P_k , (b) minimum radar SINR versus the threshold of communications SINR ξ , (c) minimum radar SINR versus the number of transmit antennas, and (d) minimum radar SINR versus the number of IRS elements.

of reflecting elements, adding more of them provides only a marginal performance improvement.

V. SUMMARY

We proposed a novel multi-IRS-aided wideband DFRC architecture with OFDM signaling in which both the LoS and NLoS are jointly processed. Contrary to prior works, this setup is more general and includes moving target in its formulation. We focused on a radar-centric design where our goal was to obtain beamformers and IRS phase shifts that are robust to Doppler shifts of the target. To address the resulting nonconvex problem, we decoupled the optimization variables into three subproblems and then solved them through an AM-based framework that was based on Dinkelbach, C-ADMM and RSD methods.

Our numerical results reveal that the proposed multi-IRS-aided DFRC system achieves a much improved performance when compared with narrowband, non-IRS and single-IRS counterparts. Meanwhile, the proposed Doppler-tolerant design scheme achieves the superior radar SINR in different Doppler slice which is crucial for moving target detection. Finally, the multi-IRS-aided wideband

DFRC provides at least 3.5 dB radar SINR enhancement over the single-IRS case at different parameter settings.

The integration of IRS and DFRC achieves better detection, wider coverage, and NLoS sensing and communications. This technology is a promising tool in future beyond 5G networks, where there is a potential to deploy IRS for aerial [72], near-field [73], and learning-driven [74] applications. All of these applications require investigation into Doppler-tolerant and wideband processing algorithms, toward which this work proposes several new techniques.

REFERENCES

- [1] T. Wei, L. Wu, K. V. Mishra, and M. R. B. Shankar, "Multiple IRS-assisted wideband dual-function radar-communication," in *IEEE International Symposium on Joint Communications & Sensing*, 2022, pp. 1–5.
- [2] M. Di Renzo, A. Zappone, M. Debbah, M.-S. Alouini, C. Yuen, J. de Rosny, and S. Tretyakov, "Smart radio environments empowered by reconfigurable intelligent surfaces: How it works, state of research, and the road ahead," *IEEE Journal on Selected Areas in Communications*, vol. 38, no. 11, pp. 2450–2525, 2020.
- [3] C. Huang *et al.*, "Reconfigurable intelligent surfaces for energy efficiency in wireless communication," *IEEE Transactions on Wireless Communications*, vol. 18, no. 8, pp. 4157–4170, 2019.

- [4] O. Özdoğan, E. Björnson, and E. G. Larsson, "Intelligent reflecting surfaces: Physics, propagation, and pathloss modeling," *IEEE Wireless Communications Letters*, vol. 9, no. 5, pp. 581–585, 2020.
- [5] Q. Wu and R. Zhang, "Towards smart and reconfigurable environment: Intelligent reflecting surface aided wireless network," *IEEE Communications Magazine*, vol. 58, no. 1, pp. 106–112, 2020.
- [6] J. A. Hodge, K. V. Mishra, and A. I. Zaghoul, "Intelligent time-varying metasurface transceiver for index modulation in 6G wireless networks," *IEEE Antennas and Wireless Propagation Letters*, vol. 19, no. 11, pp. 1891–1895, 2020.
- [7] J. C. B. Garcia, A. Sibille, and M. Kamoun, "Reconfigurable intelligent surfaces: Bridging the gap between scattering and reflection," *IEEE Journal on Selected Areas in Communications*, vol. 38, no. 11, pp. 2538–2547, 2020.
- [8] J. Liu *et al.*, "Interference analysis in reconfigurable intelligent surface-assisted multiple-input multiple-output systems," in *IEEE International Conference on Acoustics, Speech and Signal Processing*, 2021, pp. 8067–8071.
- [9] A. Aubry, A. De Maio, and M. Rosamilia, "Reconfigurable intelligent surfaces for N-LOS radar surveillance," *IEEE Transactions on Vehicular Technology*, vol. 70, no. 10, pp. 10 735–10 749, 2021.
- [10] S. Buzzi, E. Grossi, M. Lops, and L. Venturino, "Radar target detection aided by reconfigurable intelligent surfaces," *IEEE Signal Processing Letters*, vol. 28, pp. 1315–1319, 2021.
- [11] W. Lu, Q. Lin, N. Song, Q. Fang, X. Hua, and B. Deng, "Target detection in intelligent reflecting surface aided distributed MIMO radar systems," *IEEE Sensors Letters*, vol. 5, no. 3, pp. 1–4, 2021.
- [12] Z. Esmailbeig, K. V. Mishra, and M. Soltanalian, "IRS-aided radar: Enhanced target parameter estimation via intelligent reflecting surfaces," in *IEEE Sensor Array and Multichannel Signal Processing Workshop*, 2021, pp. 1–5.
- [13] C. Pan, H. Ren, K. Wang, W. Xu, M. El-kashlan, A. Nallanathan, and L. Hanzo, "Multicell MIMO communications relying on intelligent reflecting surfaces," *IEEE Transactions on Wireless Communications*, vol. 19, no. 8, pp. 5218–5233, 2020.
- [14] W. Lu, B. Deng, Q. Fang, X. Wen, and S. Peng, "Intelligent reflecting surface-enhanced target detection in MIMO radar," *IEEE Sensors Letters*, vol. 5, no. 2, pp. 1–4, 2021.
- [15] D. Xu, X. Yu, Y. Sun, D. W. K. Ng, and R. Schober, "Resource allocation for IRS-assisted full-duplex cognitive radio systems," *IEEE Transactions on Communications*, vol. 68, no. 12, pp. 7376–7394, 2020.
- [16] W. Tang, M. Z. Chen, X. Chen, J. Y. Dai, Y. Han, M. Di Renzo, Y. Zeng, S. Jin, Q. Cheng, and T. J. Cui, "Wireless communications with reconfigurable intelligent surface: Path loss modeling and experimental measurement," *IEEE Transactions on Wireless Communications*, vol. 20, no. 1, pp. 421–439, 2021.
- [17] H. Ur Rehman, F. Bellili, A. Mezghani, and E. Hossain, "Joint active and passive beamforming design for IRS-assisted multi-user MIMO systems: A VAMP-based approach," *IEEE Transactions on Communications*, vol. 69, no. 10, pp. 6734–6749, 2021.
- [18] Q. Wu and R. Zhang, "Joint active and passive beamforming optimization for intelligent reflecting surface assisted SWIPT under QoS constraints," *IEEE Journal on Selected Areas in Communications*, vol. 38, no. 8, pp. 1735–1748, 2020.
- [19] Z. Zhou, N. Ge, Z. Wang, and L. Hanzo, "Joint transmit precoding and reconfigurable intelligent surface phase adjustment: A decomposition-aided channel estimation approach," *IEEE Transactions on Communications*, vol. 69, no. 2, pp. 1228–1243, 2021.
- [20] S. Abeywickrama, R. Zhang, Q. Wu, and C. Yuen, "Intelligent reflecting surface: Practical phase shift model and beamforming optimization," *IEEE Transactions on Communications*, vol. 68, no. 9, pp. 5849–5863, 2020.
- [21] A. Elzanaty, A. Guerra, F. Guidi, and M.-S. Alouini, "Reconfigurable intelligent surfaces for localization: Position and orientation error bounds," *IEEE Transactions on Signal Processing*, vol. 69, pp. 5386–5402, 2021.
- [22] X. Yu, D. Xu, Y. Sun, D. W. K. Ng, and R. Schober, "Robust and secure wireless communications via intelligent reflecting surfaces," *IEEE Journal on Selected Areas in Communications*, vol. 38, no. 11, pp. 2637–2652, 2020.
- [23] Q. Cao, H. Zhang, Z. Shi, H. Wang, Y. Fu, G. Yang, and S. Ma, "Outage performance analysis of HARQ-aided multi-RIS systems," in *IEEE Wireless Communications and Networking Conference*, 2021, pp. 1–6.
- [24] W. Mei and R. Zhang, "Joint base station-IRS-user association in multi-IRS-aided wireless network," in *IEEE Global Communications Conference*, 2020, pp. 1–6.
- [25] M. A. Saeidi, M. J. Emadi, H. Masoumi, M. R. Mili, D. W. K. Ng, and I. Krikidis, "Weighted sum-rate maximization for multi-IRS-assisted full-duplex systems with hardware impairments," *IEEE Transactions on Cognitive Communications and Networking*, vol. 7, no. 2, pp. 466–481, 2021.
- [26] B. Zheng, C. You, and R. Zhang, "Double-IRS assisted multi-user MIMO: Cooperative passive beamforming design," *IEEE Transactions on Wireless Communications*, vol. 20, no. 7, pp. 4513–4526, 2021.
- [27] Z. Li, M. Hua, Q. Wang, and Q. Song, "Weighted sum-rate maximization for multi-IRS aided cooperative transmission," *IEEE Wireless Communications Letters*, vol. 9, no. 10, pp. 1620–1624, 2020.
- [28] W. Mei and R. Zhang, "Cooperative beam routing for multi-IRS aided communication," *IEEE Wireless Communications Letters*, vol. 10, no. 2, pp. 426–430, 2021.
- [29] Y. He, Y. Cai, H. Mao, and G. Yu, "RIS-assisted communication radar coexistence: Joint beamforming design and analysis," *IEEE Journal on Selected Areas in Communications*, 2022, in press.
- [30] Z.-M. Jiang, M. Rihan, P. Zhang, L. Huang, Q. Deng, J. Zhang, and E. M. Mohamed, "Intelligent reflecting surface aided dual-function radar and communication system," *IEEE Systems Journal*, vol. 16, no. 1, pp. 475–486, 2022.
- [31] X. Wang, Z. Fei, J. Guo, Z. Zheng, and B. Li, "RIS-assisted spectrum sharing between MIMO radar and MU-MISO communication systems," *IEEE Wireless Communications Letters*, vol. 10, no. 3, pp. 594–598, 2021.
- [32] R. Liu, M. Li, Y. Liu, Q. Wu, and Q. Liu, "Joint transmit waveform and passive beamforming design for RIS-aided DFRC systems," *IEEE Journal of Selected Topics in Signal Processing*, pp. 1–15, 2022.
- [33] Z. Zhu, Z. Li, Z. Chu, G. Sun, W. Hao, P. Xiao, and I. Lee, "Intelligent reflecting surface assisted integrated sensing and communications for mmWave channels," *arXiv preprint arXiv:2202.00552*, 2022.
- [34] M. Hua, Q. Wu, C. He, S. Ma, and W. Chen, "Joint active and passive beamforming design for IRS-aided radar-communication," *arXiv preprint arXiv:2203.14532*, 2022.
- [35] X. Wang, Z. Fei, Z. Zheng, and J. Guo, "Joint waveform design and passive beamforming for RIS-assisted dual-functional radar-communication system," *IEEE Transactions on Vehicular Technology*, vol. 70, no. 5, pp. 5131–5136, 2021.
- [36] X. Wang, Z. Fei, J. Huang, and H. Yu, "Joint waveform and discrete phase shift design for RIS-assisted integrated sensing and communication system under cramer-rao bound constraint," *IEEE Transactions on Vehicular Technology*, vol. 71, no. 1, pp. 1004–1009, 2022.
- [37] S. Buzzi, E. Grossi, M. Lops, and L. Venturino, "Foundations of MIMO radar detection aided by reconfigurable intelligent surfaces," *IEEE Transactions on Signal Processing*, pp. 1–1, 2022.
- [38] F. Wang, H. Li, and J. Fang, "Joint active and passive beamforming for IRS-assisted radar," *IEEE Signal Processing Letters*, vol. 29, pp. 349–353, 2022.
- [39] A. Aubry, A. De Maio, and M. Rosamilia, "RIS-aided radar sensing in N-LOS environment," in *IEEE International Workshop on Metrology for Aerospace*, 2021, pp. 277–282.
- [40] S. K. Dehkordi and G. Caire, "Reconfigurable propagation environment for enhancing vulnerable road users' visibility to automotive radar," in *IEEE Intelligent Vehicles Symposium*, 2021, pp. 1523–1528.
- [41] E. Cisija, A. M. Ahmed, A. Sezgin, and H. Wymeersch, "RIS-aided mmWave MIMO radar system for adaptive multi-target localization," in *IEEE Statistical Signal Processing Workshop*, 2021, pp. 196–200.
- [42] B. Watson and J. R. Guerci, *Non-line-of-sight radar*. Artech House, 2019.
- [43] S. Wei, J. Wei, X. Liu, M. Wang, S. Liu, F. Fan, X. Zhang, J. Shi, and G. Cui, "Nonline-of-sight 3-D imaging using millimeter-wave radar," *IEEE Transactions on Geoscience and Remote Sensing*, vol. 60, pp. 1–18, 2022.
- [44] R. S. Prasobh Sankar, B. Deepak, and S. P. Chepuri, "Joint communication and radar sensing with reconfigurable intelligent surfaces," in *IEEE International Workshop on Signal Processing Advances in Wireless Communications*, 2021, pp. 471–475.
- [45] A. M. Elbir, K. V. Mishra, M. R. B. Shankar, and S. Chatzinotas, "The rise of intelligent reflecting surfaces in integrated sensing and communications paradigms," *arXiv preprint arXiv:2204.07265*, 2022.
- [46] Y. Li and A. Petropulu, "Dual-function radar-communication system aided by intelligent reflecting surfaces," *arXiv preprint arXiv:2204.04721*, 2022.
- [47] H. Du, J. Kang, D. Niyato, J. Zhang, and D. I. Kim, "Reconfigurable intelligent surface-aided joint radar and covert communications: Fundamentals, optimization, and challenges," *arXiv preprint arXiv:2203.02704*, 2022.

- [48] K. V. Mishra, M. R. B. Shankar, V. Koivunen, B. Ottersten, and S. A. Vorobyov, "Toward millimeter-wave joint radar communications: A signal processing perspective," *IEEE Signal Processing Magazine*, vol. 36, no. 5, pp. 100–114, 2019.
- [49] S. H. Dokhanchi, M. R. B. Shankar, K. V. Mishra, and B. Ottersten, "A mmWave automotive joint radar-communications system," *IEEE Transactions on Aerospace and Electronic Systems*, vol. 55, no. 3, pp. 1241–1260, 2019.
- [50] L. Wu, K. V. Mishra, M. R. B. Shankar, and B. Ottersten, "Resource allocation in heterogeneously-distributed joint radar-communications under asynchronous Bayesian tracking framework," *IEEE Journal on Selected Areas in Communications*, 2022, in press.
- [51] F. Liu, C. Masouros, A. P. Petropulu, H. Griffiths, and L. Hanzo, "Joint radar and communication design: Applications, state-of-the-art, and the road ahead," *IEEE Transactions on Communications*, vol. 68, no. 6, pp. 3834–3862, 2020.
- [52] A. Hassaniien *et al.*, "Dual-function radar-communications: Information embedding using sidelobe control and waveform diversity," *IEEE Transactions on Signal Processing*, vol. 64, no. 8, pp. 2168–2181, 2016.
- [53] S. Fang, G. Chen, P. Xu, J. Tang, and J. A. Chambers, "SINR maximization for RIS-assisted secure dual-function radar communication systems," in *IEEE Global Communications Conference*, 2021, pp. 01–06.
- [54] K. V. Mishra, A. Chattopadhyay, S. S. Acharjee, and A. P. Petropulu, "OptM3Sec: Optimizing multicast IRS-aided multiantenna DFRC secrecy channel with multiple eavesdroppers," in *IEEE International Conference on Acoustics, Speech and Signal Processing*, 2022, pp. 9037–9041.
- [55] W. Liu and S. Weiss, *Wideband beamforming: Concepts and techniques*. John Wiley & Sons, 2010.
- [56] S. Ma, W. Shen, J. An, and L. Hanzo, "Wideband channel estimation for IRS-aided systems in the face of beam squint," *IEEE Transactions on Wireless Communications*, vol. 20, no. 10, pp. 6240–6253, 2021.
- [57] Z. Cheng, S. Shi, Z. He, and B. Liao, "Transmit sequence design for dual-function radar-communication system with one-bit DACs," *IEEE Transactions on Wireless Communications*, vol. 20, no. 9, pp. 5846–5860, 2021.
- [58] Z. Cheng, Z. He, and B. Liao, "Hybrid beamforming design for OFDM dual-function radar-communication system," *IEEE Journal of Selected Topics in Signal Processing*, vol. 15, no. 6, pp. 1455–1467, 2021.
- [59] S. Sun, K. V. Mishra, and A. P. Petropulu, "Target estimation by exploiting low rank structure in widely separated MIMO radar," in *IEEE Radar Conference*, 2019, pp. 1–6.
- [60] H. Li *et al.*, "Dynamic hybrid beamforming with low-resolution PSs for wideband mmWave MIMO-OFDM systems," *IEEE Journal on Selected Areas in Communications*, vol. 38, no. 9, pp. 2168–2181, 2020.
- [61] E. Vlachos, G. C. Alexandropoulos, and J. Thompson, "Wideband MIMO channel estimation for hybrid beamforming millimeter wave systems via random spatial sampling," *IEEE Journal of Selected Topics in Signal Processing*, vol. 13, no. 5, pp. 1136–1150, 2019.
- [62] J. He, H. Wymeersch, and M. Juntti, "Channel estimation for RIS-aided mmWave MIMO systems via atomic norm minimization," *IEEE Transactions on Wireless Communications*, vol. 20, no. 9, pp. 5786–5797, 2021.
- [63] A. Aubry, A. De Maio, and M. M. Naghsh, "Optimizing radar waveform and Doppler filter bank via generalized fractional programming," *IEEE Journal of Selected Topics in Signal Processing*, vol. 9, no. 8, pp. 1387–1399, 2015.
- [64] D. P. Bertsekas, "Nonlinear programming," *Journal of the Operational Research Society*, vol. 48, no. 3, pp. 334–334, 1997.
- [65] A. Charnes and W. W. Cooper, "Programming with linear fractional functionals," *Naval Research Logistics Quarterly*, vol. 9, no. 3–4, pp. 181–186, 1962.
- [66] Y. Huang and D. P. Palomar, "Rank-constrained separable semidefinite programming with applications to optimal beamforming," *IEEE Transactions on Signal Processing*, vol. 58, no. 2, pp. 664–678, 2010.
- [67] Z.-Q. Luo, W.-K. Ma, A. M.-C. So, Y. Ye, and S. Zhang, "Semidefinite relaxation of quadratic optimization problems," *IEEE Signal Processing Magazine*, vol. 27, no. 3, pp. 20–34, 2010.
- [68] K. B. Petersen and M. S. Pedersen, *The matrix cookbook*. Technical University of Denmark, 2012.
- [69] J. Yang, G. Cui, X. Yu, and L. Kong, "Dual-use signal design for radar and communication via ambiguity function sidelobe control," *IEEE Transactions on Vehicular Technology*, vol. 69, no. 9, pp. 9781–9794, 2020.
- [70] M. Grant, S. Boyd, and Y. Ye, "CVX: MATLAB software for disciplined convex programming," 2009.
- [71] G. Duggal, S. Vishwakarma, K. V. Mishra, and S. S. Ram, "Doppler-resilient 802.11ad-based ultrashort range automotive joint radar-communications system," *IEEE Transactions on Aerospace and Electronic Systems*, vol. 56, no. 5, pp. 4035–4048, 2020.
- [72] H. Lu, Y. Zeng, S. Jin, and R. Zhang, "Aerial intelligent reflecting surface: Joint placement and passive beamforming design with 3D beam flattening," *IEEE Transactions on Wireless Communications*, vol. 20, no. 7, pp. 4128–4143, 2021.
- [73] D. Dardari and N. Decarli, "Holographic communication using intelligent surfaces," *IEEE Communications Magazine*, vol. 59, no. 6, pp. 35–41, 2021.
- [74] A. M. Elbir and K. V. Mishra, "A survey of deep learning architectures for intelligent reflecting surfaces," *arXiv preprint arXiv:2009.02540*, 2020.